



# In situ strontium and sulfur isotope investigation of the Ni-Cu-(PGE) sulfide ore-bearing Kevitsa intrusion, northern Finland

Kirsi Luolavirta<sup>1</sup> · Eero Hanski<sup>1</sup> · Wolfgang Maier<sup>2</sup> · Yann Lahaye<sup>3</sup> · Hugh O'Brien<sup>3</sup> · Frank Santaguida<sup>4</sup>

Received: 26 May 2017 / Accepted: 4 January 2018 / Published online: 25 January 2018  
© Springer-Verlag GmbH Germany, part of Springer Nature 2018

## Abstract

The ~2.06-Ga Kevitsa mafic-ultramafic intrusion in northern Finland hosts a large disseminated Ni-Cu-PGE deposit. The deposit occurs in the ultramafic olivine-pyroxene cumulates and shows a range in Ni tenors varying from 4–7 wt% (regular ore) to > 10 wt% (Ni-PGE ore). There are also a metal-poor sulfide mineralization (false ore) and contact mineralization that are uneconomic (Ni tenor < 4 wt%). The obtained  $^{87}\text{Sr}/^{86}\text{Sr}_{(i)}$  values of the Kevitsa ultramafic cumulates are highly radiogenic (> 0.7045) in comparison to the estimated depleted mantle Sr isotope ratio of ~0.702 at 2.06 Ga. The sulfur  $\delta^{34}\text{S}$  values are generally higher than +2‰, which together with the Sr isotope data imply involvement of crustal material in the genesis of the Kevitsa intrusion and its ores. The  $^{87}\text{Sr}/^{86}\text{Sr}_{(i)}$  values obtained from the ore-bearing domain of the intrusion show stratigraphic variation and exceed 0.7050, with the maximum value reaching up to 0.7109. In contrast, in rocks around the ore domain, the initial Sr isotope compositions remain more or less constant (0.7047–0.7060) throughout the intrusive stratigraphy. The isotope data suggest that the ore-bearing domain of the intrusion represents a dynamic site with multiple injections of variably contaminated magma, whereas the surrounding part of the intrusion experienced a less vigorous emplacement history. No correlation is observed between the strontium and sulfur isotope compositions. This is explained by bulk assimilation of the silicate magma in a deeper staging magma chamber and variable assimilation of sulfur during magma transport into the Kevitsa magma chamber. The low level of metals in false ore and the Ni-depleted nature of its olivine suggest that some sulfides may have precipitated and deposited in the feeder conduit during the initial stage of magma emplacement. Cannibalization of early-formed sulfides by later magma injections may have been important in the formation of the economic ore deposit.

**Keywords** Strontium isotopes · Sulfur isotopes · Ni-Cu-PGE sulfide ore · Kevitsa intrusion · Central Lapland greenstone belt

## Introduction

The evolutionary histories of mafic-ultramafic intrusive bodies may involve complex episodes of magma replenishment,

---

Editorial handling: P. Eilu

**Electronic supplementary material** The online version of this article (<https://doi.org/10.1007/s00126-018-0792-6>) contains supplementary material, which is available to authorized users.

✉ Kirsi Luolavirta  
kirsi.luolavirta@student oulu.fi

<sup>1</sup> Oulu Mining School, University of Oulu, P.O. Box 3000, FI-90014 Oulu, Finland

<sup>2</sup> The School of Earth and Ocean Sciences, Cardiff University, Cardiff CF10 3AT, UK

<sup>3</sup> Geological Survey of Finland, 02151 Espoo, Finland

<sup>4</sup> First Cobalt Corb, Suite 201, 140 Yonge Street, Toronto, Canada

magma mixing and mingling, contamination, crystal fractionation, and postcumulus processes (e.g., DePaolo 1985; Sparks et al. 1985; Meyer and Wilson 1999; Namur et al. 2010). Whole-rock chemistry and mineral compositions are widely applied to interpret magmatic histories of intrusive bodies (e.g., Seat et al. 2007; Pang et al. 2009; Namur et al. 2010). Where these compositions change due to crystal fractionation, radiogenic or stable isotope ratios remain unaffected in closed system processes but may change due to addition of crustal contaminants or influx of magmas of distinct lineage into magma chambers. Consequently, isotopes have the advantage of identifying involvement of isotopically distinct magmas in the generation of igneous rock suites.

In situ LA-MC-ICP-MS analysis is an effective method to determine the Sr isotope composition of plagioclase grains, potentially revealing variations in the magma composition from which the plagioclase crystallized. Grain-scale studies

have been used to identify open magma chambers (Liu et al. 2014), to identify chemically distinct magmas and mixing of either magmas or minerals (Tepley et al. 1999; Seabrook et al. 2005; Yang et al. 2013a; Chen et al. 2016), and to reveal crustal contamination (Tepley and Davidson 2003). Hence, isotopes provide a tool to unravel processes operating during filling of magma chambers, including those related to sulfide ore formation in mineralized intrusions.

The Ni-Cu-(PGE) sulfide ore-bearing Kevitsa intrusion is one of the manifestations of the widespread Paleoproterozoic mafic magmatism in the Central Lapland greenstone belt, northern Finland (Hanski and Huhma 2005). Other roughly coeval magmatic sulfide mineralization is represented by the nearby Sakatti Cu-Ni-PGE deposit occurring in a small subvolcanic peridotite body (Brownscombe et al. 2015) and the komatiite-hosted Lomalampi PGE-(Ni-Cu) deposit (Törmänen et al. 2016). The Kevitsa Ni-Cu-(PGE) ore occurs in the central part of the ultramafic portion of the intrusion, whereas magmatic sulfide segregations are more commonly found at the base of differentiated mafic-ultramafic intrusions (e.g., Barnes and Lightfoot 2005). The deposit is made up of low-grade disseminated sulfides with current measured, indicated, and inferred mineral resources of 166 Mt at 0.22% Ni, 0.35% Cu, 0.13 g/t Pt, and 0.08 g/t Pd (data available at [www.boliden.com](http://www.boliden.com)). The metal content of sulfides shows an unusually large variation with their Ni tenors covering a range from ~4 up to 40 wt% (Mutanen 1997; Yang et al. 2013b).

According to the interpretations by Mutanen (1997), the Kevitsa intrusion represents differentiation of a single batch of basaltic magma, and in part, lithological and chemical variations reflect variable degrees of in situ contamination with material from pelitic metasedimentary and mafic-ultramafic volcanogenic rocks. More recently, the injection of multiple magma pulses has been considered a more plausible explanation for the lithological and compositional variability within the ore domain and for the formation of the sulfide ores (Gregory et al. 2011; Luolavirta et al. 2018b). A dynamic magma plumbing system could enable sulfide liquid to interact with a large volume of silicate magma, leading to an increase in the chalcophile element contents of the sulfides. Such an open-system behavior has been emphasized by Naldrett (1999, 2011) as one of the fundamental aspects in the formation of magmatic sulfide ores and has been regarded as plausible in various well-known ore deposits, such as Voisey's Bay (Li and Naldrett 1999), Jinchuan (Song et al. 2009), Noril'sk-Talnakh (Li et al. 2003), and Uitkomst (Li et al. 2002).

Another key process in the formation of magmatic sulfide deposits is segregation of an immiscible sulfide liquid (e.g., Naldrett 2004). Sulfide saturation of mafic magma can be achieved via various mechanisms involving changes in magma compositions or P-T conditions (see Li and Ripley 2005

and Ripley and Li 2013 for reviews); yet, incorporation of external sulfur is generally considered most important (e.g., Ripley and Li 2013; Keyes and Lightfoot 2010). The evidence for the presence of external sulfur is well-documented from many Ni-Cu-PGE sulfide deposits, such as Noril'sk (Li et al. 2003; Malitch et al. 2014), Voisey's Bay (Ripley et al. 1999, 2002), Jinchuan (Ripley et al. 2005; Duan et al. 2016), and Pechenga (Barnes et al. 2001), with the most convincing argument being the nonmantle-like S isotope signatures. However, some large sulfide deposits, notably Nebo-Babel (Seat et al. 2009), lack definite crustal S isotopic signatures, and hence, the necessity of external sulfur in generating a sulfide deposit is debatable.

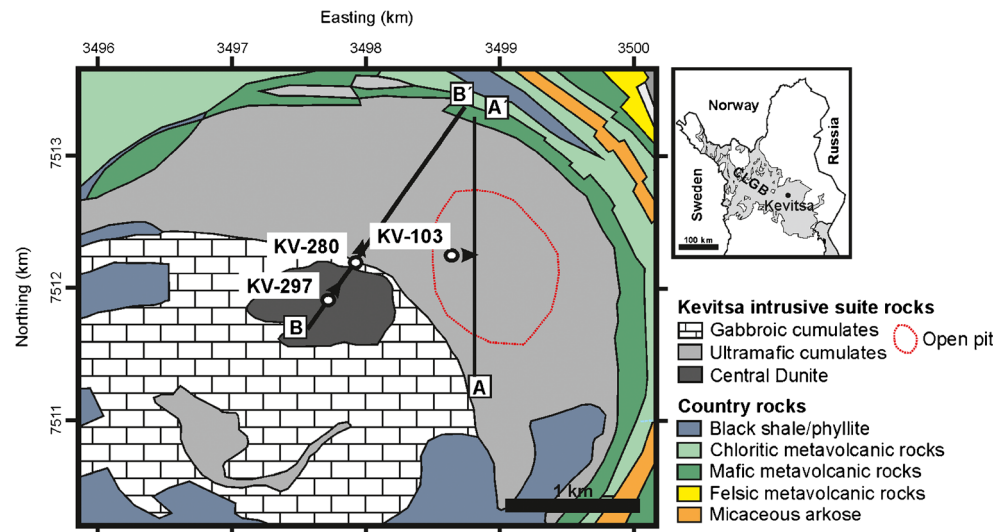
In this study, we report in situ Sr isotope data for plagioclase and in situ S isotope data for sulfides from the Kevitsa intrusion in order to assess the nature of magma chamber processes and the role of crustal contamination in the formation of the Kevitsa intrusion and its ore deposit. Interestingly, the range of isotopic compositions and the isotope stratigraphy turned out to be markedly different in different parts of the intrusion.

## Geological setting of the Kevitsa intrusion

The ca. 2058 ± 4-Ma Kevitsa mafic-ultramafic intrusion is located in the Central Lapland greenstone belt (CLGB) in northern Finland (Mutanen 1997; Mutanen and Huhma 2001; Fig. 1). The CLGB is mainly composed of Paleoproterozoic komatiitic to rhyolitic metavolcanic rocks, mafic-ultramafic intrusions, and sedimentary rocks with an evolutionary history ranging from ca. 2.5 to 1.8 Ga. The geology of the CLGB is summarized by Hanski and Huhma (2005). A number of mafic-ultramafic intrusive bodies and volcanic rocks occur in the vicinity of the Kevitsa intrusion, including the large 2.44-Ga Koitelainen layered intrusion (Mutanen and Huhma 2001) and the Cu-Ni-PGE ore-bearing Sakatti intrusion (Brownscombe et al. 2015).

The CLGB is divided into six stratigraphic groups which are from oldest to youngest: Salla, Onkamo (currently Kuusamo Group); Sodankylä, Savukoski, Kittilä (Kittilä suite); and Kumpu Groups (Hanski and Huhma 2005; Luukas et al. 2017). The Kevitsa intrusion is hosted by the Savukoski Group volcano-sedimentary sequence consisting of interlayered phyllites, graphitic black shales, and mafic to ultramafic volcanogenic rocks (Lehtonen et al. 1998; Hanski et al. 2001a; Hanski and Huhma 2005). The volcano-sedimentary country rocks are locally recrystallized to a fine-grained hornfels aureole around the intrusion. The metavolcanic rocks and, in particular, the black shales, may contain high quantities of sulfides.

**Fig. 1** Geologic map of the Kevitsa intrusion and location of the sampled drill cores and cross sections of Fig. 2. Location of the Ni-Cu-(PGE) deposit is denoted by the outline of the open pit



## Kevitsa intrusion and its ore types

The Kevitsa intrusion is composed of an approximately 1.5-km-thick ultramafic lower part and a gabbroic upper part with a minor amount of granophyre on top (Mutanen 1997; Fig. 1). The maximum thickness of the gabbroic succession at the current erosional level exceeds 500 m. In addition, dunitic rocks occur as inclusions within the Kevitsa intrusion and as a separate intrusive body (Central Dunite) in close association with the Kevitsa intrusive successions (Mutanen 1997; Yang et al. 2013b; Luolavirta et al. 2018a) (Fig. 1).

## Rock types

At the bottom of the Kevitsa intrusion, there is a basal series comprising pyroxenite and gabbro. The overlying ultramafic cumulates include olivine pyroxenites (OLPX), plagioclase-bearing (olivine) websterites (pOLWB), and pyroxenites (PX) (Fig. 2). The olivine pyroxenites (more precisely olivine websterites and olivine clinopyroxenites) represent the most abundant rock type and are composed of cumulus olivine (10–30%), clinopyroxene (65–85%), and oikocrystic orthopyroxene (0–15%), showing ad- to mesocumulate textures (Fig. 3a, b). The pyroxenites contain less than 5% olivine (Fig. 3c). Accessory minerals include magnetite, intercumulus plagioclase, sulfides, and locally phlogopite, hornblende, ilmenite, and apatite. Plagioclase-bearing olivine websterites can be distinguished from typical olivine pyroxenites and pyroxenites by their higher contents of plagioclase (15–25%) and orthopyroxene (15–30%). In pOLWB, plagioclase occurs largely as an intercumulus phase defining an orthocumulate texture (Fig. 3d, e). Olivine can be one of the major constituents of pOLWB (up to 15%) or absent. Hornblende, phlogopite, magnetite, and sulfides are common accessory minerals. Fine-grained gabbros (microgabbros) with gradational

contacts are found in close association with pOLWB and are considered as part of the pOLWB zones. Hence, we use the term pOLWB or pOLWB zone as a lithological unit including microgabbros.

Clinopyroxene and olivine are the prevalent constituents throughout the ultramafic zone, being generally subhedral and rather equal in size (~0.5–1.5 mm). Orthopyroxene is oikocrystic (~2–5 mm), enclosing rounded to anhedral grains of olivine, clinopyroxene, and magnetite. In olivine pyroxenites and pyroxenites, plagioclase occurs as a low-mode intercumulus phase. In pOLWB, plagioclase occupies large intercumulus domains as irregularly shaped individual grains up to 5 mm in size, which may enclose olivine and clinopyroxene. Aggregates of smaller anhedral/subhedral plagioclase crystals occur as well.

The Central Dunite is composed of olivine-chromite cumulates, with its modal mineralogy varying from dunite to wehrlite and feldspathic wehrlite. The dunite body shows a chemical affinity to the picritic basalts of the Savukoski Group as well as to the Kevitsa olivine-pyroxene cumulates and has been regarded as representing an initial stage of the formation of the Kevitsa intrusive suite rocks (Luolavirta et al. 2018a). The ore-bearing domain of the ultramafic zone is characterized by numerous rafts of dunitic rocks (up to several tens of meters in size) and komatiitic xenoliths. Pelitic xenoliths are rare within the ultramafic zone and tend to be found near the basal contact of the intrusion.

## Internal stratigraphy

In terms of lithological variation, the cumulate stratigraphy of the ultramafic rocks constituting the ore-bearing domain and the surrounding intrusion are hard to correlate. The ore domain is characterized by numerous dunitic and komatiitic inclusions, discontinuous zones of pOLWB within the OLPX

**Fig. 2** **a** S-N (A–A′) and **b** SE-NE (B–B′) cross sections across the Kevitsa intrusion showing the broad outlines of the Ni-Cu-(PGE) ore body (>0.15% Ni) and false ore bodies around the ore domain (<0.1% Ni). For locations of the profiles, see Fig. 1

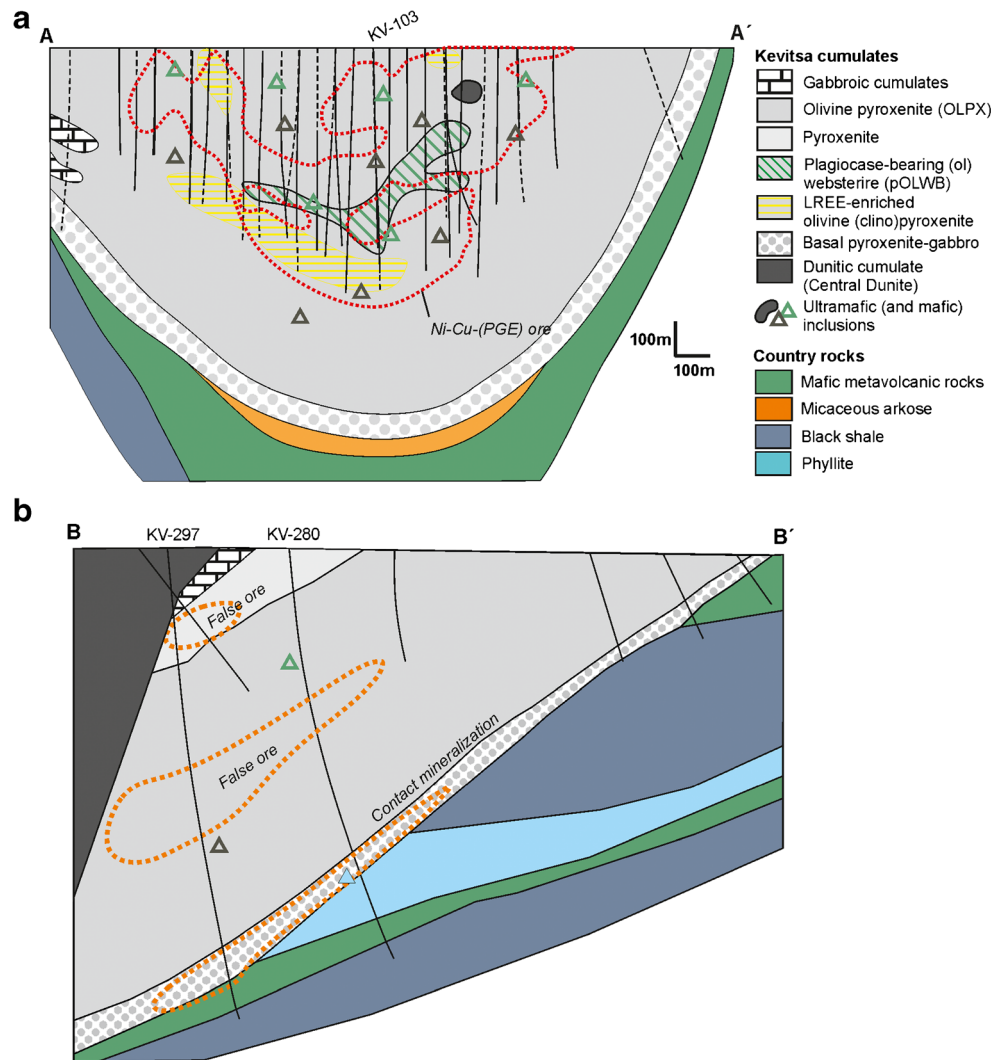


(Fig. 2a) and stratigraphic fluctuations in whole-rock and mineral compositions. Around the ore domain, the rocks appear far more homogeneous and a simple stratigraphy with a typical evolutionary trend from basal series rocks via olivine pyroxenites and pyroxenites is observed (Fig. 2b). The relationship between the gabbroic zone and the ultramafic part of the Kevitsa intrusion is not well constrained. Overall, in the south, the contact appears steeply dipping and interfingering.

### The deposit and ore types

The Kevitsa Ni-Cu-(PGE) deposit is hosted by olivine pyroxenites in the central part of the ultramafic zone of the intrusion (Fig. 2a). The mineralization is made up of low-grade disseminated sulfides, with the whole-rock sulfur content typically being below 3 wt%. The low grades are compensated by the large dimensions of the ore body: it extends along the northwest axis for more than 1200 m, has a width of ~500 m and exceeds to a depth of up to 800 m. The ore body is irregular in

shape and consists of several mineralized domains with variable ore grades.

Based mainly on the Ni tenor, four ore types were recognized by Mutanen (1997): “regular,” “Ni-PGE,” “false,” and contact mineralization. The regular and Ni-PGE ore (Ni-Cu-(PGE) ore) comprise the economic resources, of which the regular ore type covers ~95% by volume (Santaguida et al. 2015). The regular ore type generally has a Ni tenor in the range of 4–7%, with Ni/Cu ratio falling below 1 and the PGE content varying from “low” (~100 ppb of Pt) to high (~750 ppb of Pt). The Ni-PGE ore occurs as lens-like discontinuous bodies and is characterized by a high Ni tenor of >10%, low copper, and high PGE contents (400 to 3000 ppb of Pt). In the preliminary characterization of the ore types by Mutanen (1997), the term “transitional ore” was also used to an ore type with an intermediate composition between the regular and Ni-PGE ore. However, based on the chemical affinity of the transitional ore toward the Ni-PGE ore (Hanski et al. 1997, discussed below), the transitional ore can be considered lower-grade Ni-PGE ore. The uneconomic mineralization that

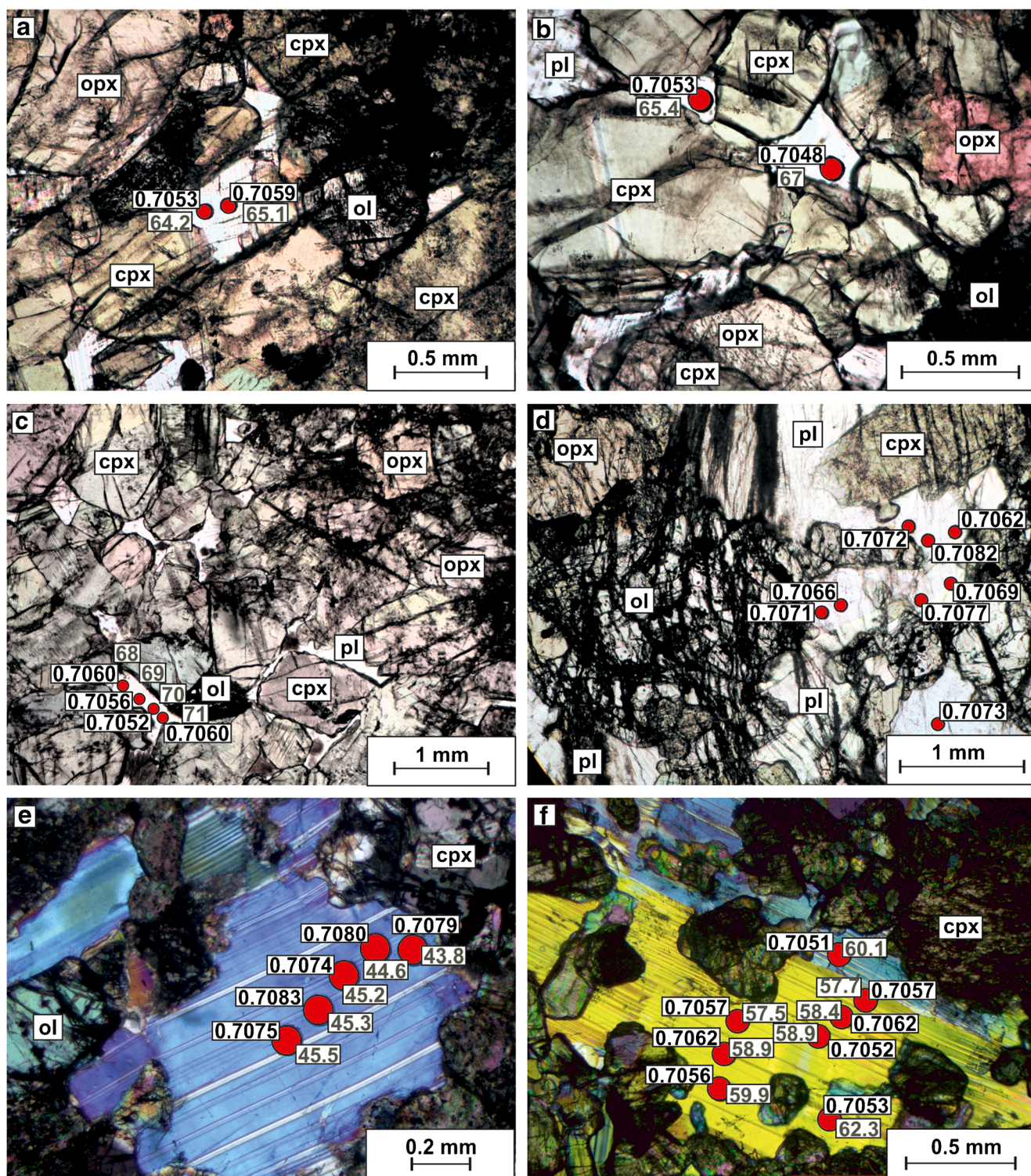


**Fig. 3** Photomicrographs of rocks from the Kevitsa ultramafic zone, showing laser spot positions as red circles and  $Sr_{(i)}$  ratios with corresponding An contents in plagioclase. **a, b** Olivine pyroxenite. **c** Pyroxenite. **d–f** Plagioclase-bearing (ol) websterite

is called false ore has a low Ni tenor (0.5–4 wt%) and low Pd and Pt contents, ranging from few tens of ppb to values below the detection limit of 10 ppb. The contact mineralization can locally comprise semimassive sulfides but shows very low metal contents (Ni tenor 1–2 wt%). It is worth emphasizing

that there exists a continuous range of ore compositions with two broad compositional trends from the regular ore: one toward ores very rich in Ni (and PGE) and low in Cu and the other toward mineralized rocks almost totally devoid of Ni, Cu, and PGE.

There is a clear relationship between the metal tenors of the different ore types and their sulfide mineral assemblages. The dominant ore minerals are pentlandite and chalcopyrite in the regular ore type and pentlandite, millerite, and heazlewoodite in the Ni-PGE ore type. The false ore and contact mineralization are dominated by pyrrhotite. The sulfides occur together with a small amount of magnetite in the interstitial spaces between olivine and pyroxene grains. Besides the well-developed magmatic textures of the sulfides, the magmatic origin of the mineralization is reflected, for example, in positive correlations between nickel, copper, and sulfur contents as well as between platinum and palladium concentrations (not shown). Pd/Pt ratios for false ore, regular ore, and Ni-PGE ore are similar ( $\sim 0.6$ ; Le Vaillant et al. 2016). Effects of hydrothermal alteration to the Kevitsa sulfide ore has recently been discussed by Le Vaillant et al. (2016) who argue that of the base metals, copper (and Au) may have been locally redistributed, but to what extent is not well established.

Besides metal tenors, the ore types show differences in their REE contents and isotope compositions. The most intriguing mineralization type is the Ni-PGE ore, which has abnormally high contents of Ni, not only in the sulfides, but also in the primary silicates (olivine and clinopyroxene), being in this sense very “primitive” (Mutanen 1997; Yang et al. 2013b; Luolavirta et al. 2018b). Yet, this ore type has significantly LREE-enriched chondrite-normalized REE patterns ( $Ce_N/Yb_N \sim 7$ , Hanski et al. 1997; Luolavirta et al. 2018b) and records low initial  $\epsilon_{Nd}$  ( $-6.4$ ; Huhma et al. 2017 in review) (Fig. 4). Furthermore, Luolavirta et al. (2018b) demonstrated that there is a mineralogical difference between the ore types, as the host rocks to the Ni-PGE ore type tend to be

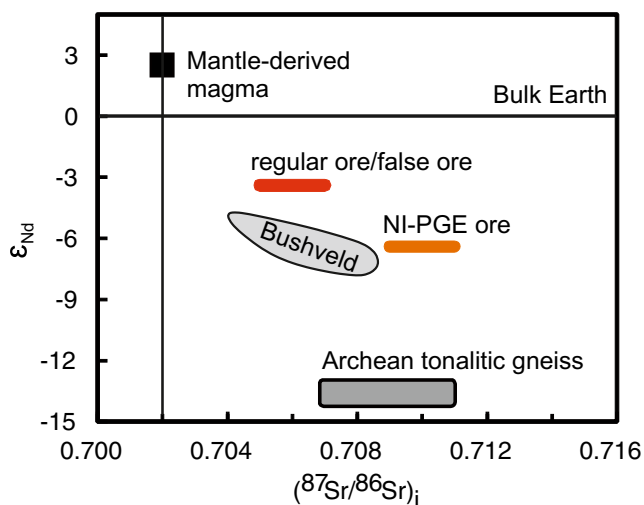


**Fig. 4**  $\epsilon_{Nd}$  vs.  $^{87}Sr/^{86}Sr_{(i)}$  diagram showing compositions of the Kevitsa false, regular, and Ni-PGE ore types.  $\epsilon_{Nd}$  data for Kevitsa ores from Huhma et al. (2017, in review) and Sr isotopic data from the present study. Field for Bushveld Lower and Main zone and mantle-derived magma after Maier et al. (2000) and for Archean tonalitic gneiss (Tojottamanselkä gneiss, 10 km north of Kevitsa) after Hanski et al. (2001b) and Kröner et al. (1981)

virtually devoid of orthopyroxene (olivine clinopyroxenites). The  $\epsilon_{Nd}$  values for regular and false ore are similar ( $-3.4$ ; Huhma et al. 2017, in review) (Fig. 4) with both of them showing mildly LREE-enriched REE patterns ( $Ce_N/Yb_N \sim 2$ ; Hanski et al. 1997; Luolavirta et al. 2018b), but they differ in terms of their S isotope compositions. Average whole-rock  $\delta^{34}S$  values of  $+3.8$ ,  $+6.1$ , and  $+8.2\%$  have been reported for regular, Ni-PGE (including the transitional ore), and false ore, respectively (Grinenko et al. 2003) (Fig. 5).

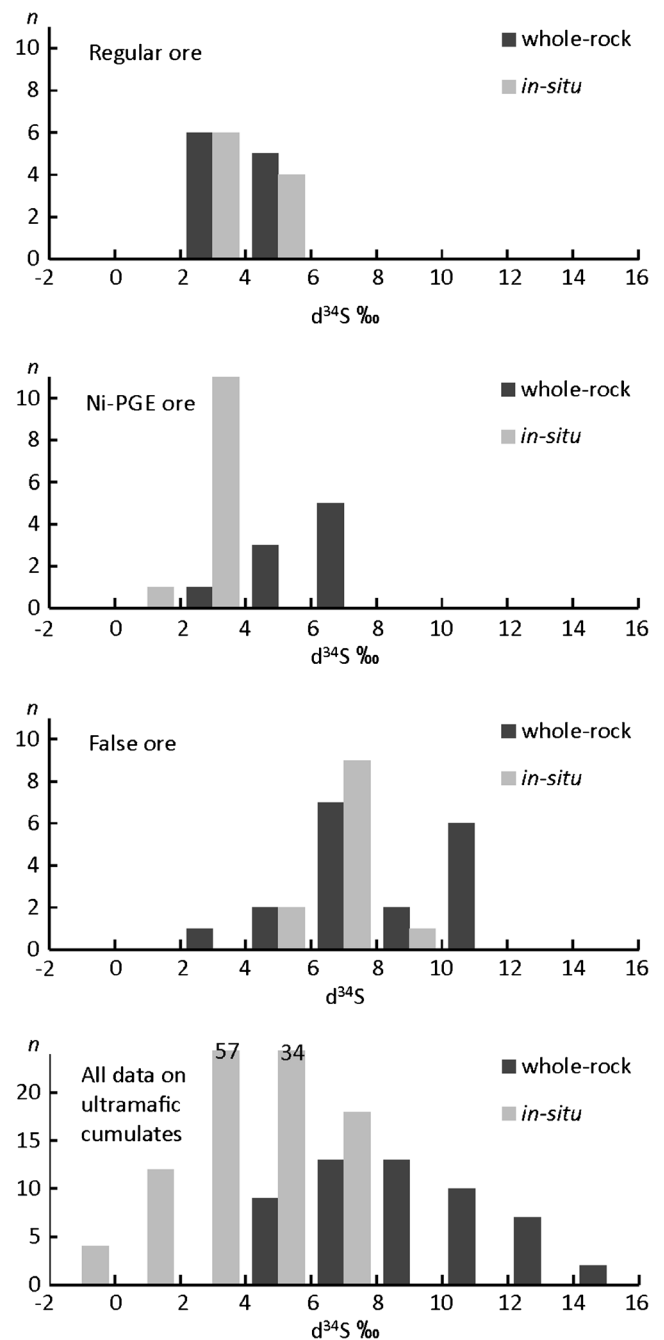


**Fig. 5** Sulfur isotopic compositions of Kevitsa ores and ultramafic rocks. Whole-rock data from Grinenko et al. (2003). In situ data from the present study

## Sampling and analytical methods

### Samples

Samples for in situ strontium and sulfur isotope analyses were collected from three drill cores to cover the stratigraphy through the ultramafic cumulate succession and to obtain isotope data from the different ore types. Drill core KV-103 represents the ore domain, being relatively deep (~750 m) and intersecting both the regular and Ni-PGE ore types. Drill cores KV-280 and KV-297 are located a few hundred meters outside the ore-bearing domain and intersect a false ore-type mineralization and contact mineralization. The compositions of major minerals (olivine, clinopyroxene, orthopyroxene) of these drill cores are discussed in another paper (Luolavirta et al. 2018b).

### Analytical methods

In situ Sr isotope analyses of plagioclase were performed by laser ablation multicollector inductively coupled plasma mass spectrometry (LA-MC-ICP-MS) using a Nu Plasma HR mass spectrometer and a Photon Machine Analyte G2 laser microprobe at the Geological Survey of Finland in Espoo. Samples were ablated in He gas (gas flows = 0.4 and 0.1 l/min) within a HelEx ablation cell (Müller et al. 2009). Strontium isotope analyses of plagioclase were made in static ablation mode employing the following parameters: beam diameter 110 µm, pulse frequency 10 Hz, and beam fluence 2.07 J/cm<sup>2</sup>. The MC-ICP-MS instrument was equipped with 9 Faraday detectors and amplifiers with 10<sup>11</sup> Ω resistors. During the laser ablation, data were collected in static mode (<sup>84</sup>Sr-Kr, <sup>85</sup>Rb, <sup>86</sup>Sr-Kr, <sup>87</sup>Rb-Sr, <sup>88</sup>Sr). Measured isotope ratios were corrected for instrument fractionation applying an exponential law and a <sup>86</sup>Sr/<sup>88</sup>Sr value of 0.1194. The isobaric interference of <sup>87</sup>Rb on <sup>87</sup>Sr was monitored and corrected using the <sup>85</sup>Rb ion signal and a value of 0.38571 for the <sup>87</sup>Rb/<sup>85</sup>Rb ratio. The isobaric interference of <sup>86</sup>Kr on <sup>86</sup>Sr was corrected using a 30-s background measurement, preceding every ablation. Strontium isotope ratios were age-corrected to 2058 Ma based on <sup>85</sup>Rb/<sup>86</sup>Sr ratios. The average total Sr signal obtained for plagioclase samples was 0.4 V. Under these conditions, 120 s of ablation is needed to obtain an internal precision of  $\leq \pm 0.00007$  (1σ). The decay constant of <sup>87</sup>Rb of  $1.3968 \times 10^{-11}$  year<sup>-1</sup> given by Rotenberg et al. (2012) was used in all calculations. The accuracy of the laser ablation protocol was verified throughout the day of measurement by repeated analysis of an in-house plagioclase standard from a megacryst of the Cameroon volcanic chain (sample Mir a; Rankenburg et al. 2004). The laser ablation parameters were similar for the samples and standard. During the course of this study, the measured <sup>87</sup>Sr/<sup>86</sup>Sr values for the standard ranged from 0.70300 to 0.70319 and averaged  $0.70310 \pm 0.00008$  (2σ, n = 30), which is similar to the TIMS value of

$0.70311 \pm 0.0001$  (2σ) obtained by Rankenburg et al. (2004). Variation in the <sup>87</sup>Sr/<sup>86</sup>Sr ratio of the plagioclase standard over the course of the study are given in Electronic supplementary material 1 (ESM 1).

In situ sulfur isotopes analyses of pyrrhotite and pyrite were performed employing the same instrument as for the Sr isotope analyses. Samples were ablated in He gas (gas flows = 0.4 and 0.1 l/min) within a HelEx ablation cell (Müller et al. 2009). Sulfur isotopes were measured at medium resolution. During the ablation, data were collected in static mode (<sup>32</sup>S, <sup>34</sup>S). Sulfide samples were ablated at a spatial resolution of 50 µm, using a laser beam fluence of 0.83 J/cm<sup>2</sup> at 5 Hz. The total S signal was typically 0.5–4.0 V. Under these conditions, after a 20-s baseline measurement, 30–40 s of ablation is needed to obtain an internal precision in <sup>34</sup>S/<sup>32</sup>S of  $\leq \pm 0.000005$  (1 SE). In-house pyrrhotite and pyrite standards were utilized for external standard bracketing and quality control of analyses. The standards used have been analyzed by gas mass spectrometry. For the quality control pyrite standard, our measured  $\delta^{34}\text{S}_{\text{CDT}}$  (‰) value is  $+6.61 \pm 0.45$  (n = 29) against the gas mass spectrometer-determined value of  $+5.8 \pm 0.3$  (‰). For pyrrhotite, these values are  $4.4 \pm 0.3$  (‰, 1σ, n = 13) and  $+4.8 \pm 0.3$  (‰, 1σ, n = 3), respectively.

Plagioclase compositions were determined using a JEOL JXA-8200 electron microprobe at the Center of Microscopy and Nanotechnology, the University of Oulu, with a standard built-in ZAF correction routine. The analytical conditions were an accelerating voltage of 15 kV and a beam current of 30 nA. Peak counting times on major elements were 60 and 30 s for the background. The whole-rock trace elements used in this study were provided by the mining company. Whole-rock major and trace element abundances were produced at an ALS geochemistry laboratory using ICP-MS/ICP-AES after four-acid near-total sample digestion and precious metals by ICP-MS/ICP-AES after fire assay preconcentration.

## Results

### Sr isotope composition of plagioclase

#### General features

Only fresh and nonfractured interstitial plagioclase grains were selected for laser ablation to minimize alteration effects to the Rb-Sr isotope system. The Rb/Sr ratios of the analyzed plagioclase grains are low and relatively constant ( $\leq 0.005$ ) indicating very little growth of radiogenic <sup>87</sup>Sr by <sup>87</sup>Rb decay since the crystallization of the Kevitsa intrusion at 2.06 Ga. As stated above, results of repeated analyses of in-house standard are within the recommended value, verifying the accuracy of our laser ablation protocol (see ESM 1). Representative isotope data with 2σ error margins and anorthite contents of

plagioclase are presented in Table 1 and the whole dataset is tabulated in Electronic supplementary material 2 (ESM 2).

It must be noted that the low mode of plagioclase restricted the number of spot analyses in OLPX and PX samples, whereas for pOLWB, a more comprehensive sampling could be conducted. Nevertheless, the measured  $^{87}\text{Sr}/^{86}\text{Sr}_{(i)}$  ratios are heterogeneous in each sample (Fig. 3), and overall, no observable correlations with An contents and  $^{87}\text{Sr}/^{86}\text{Sr}_{(i)}$  could be established. Relationships between the anorthite content and  $^{87}\text{Sr}/^{86}\text{Sr}_{(i)}$  in plagioclase are illustrated in Electronic supplementary material 3 (ESM 3).

#### Drill cores KV-297 and KV-280 (outside the ore domain)

The initial  $^{87}\text{Sr}/^{86}\text{Sr}$  ratios in the samples collected from the “unmineralized” part of the Kevitsa intrusion vary from 0.7047 to 0.7060 (Figs. 6 and 7). In one sample of false ore

(KV-280 ~ 520 m) and in the gabbro at the top of drill core KV-297, individual spot analyses show slightly higher initial ratios (0.0768 and 0.7065, respectively). However, the observed range of Sr isotope compositions remains relatively constant throughout the stratigraphy.

Overall, the An contents increase slightly from the base upwards, after which they remain constant in OLPX and then decrease toward the top of the ultramafic unit. One sample (at a depth of around 750 m in drill core KV-280) stands out in having markedly lower An contents. This sample contains abundant primary phlogopite, which is not common in other studied samples. The only cumulus plagioclase analyzed in this study is from the gabbro sample at the top of drill core KV-297. This sample shows a highly heterogeneous plagioclase composition, but the Sr isotope ratios are in the same range as in the underlying ultramafic cumulates. It appears that the cores of individual plagioclase grains record the

**Table 1** Representative in situ isotope data from plagioclase and sulfides from the Kevitsa ultramafic zone

Sample	Lithology	$^{87}\text{Rb}/^{86}\text{Sr}$	$^{87}\text{Sr}/^{86}\text{Sr}$	$^{87}\text{Sr}/^{86}\text{Sr}_{(i)}$	$2\sigma$	An	$\delta^{34}\text{S}\text{‰}$	$2\sigma$		
KV-280-74.45	PX	0.0049	0.7058	0.7056	0.00014	68.7				
		0.0061	0.7058	0.7056	0.00014	51.7				
		0.0071	0.7057	0.7055	0.00015	51.4				
KV-297-391.95	OLPX	0.0020	0.7056	0.7056	0.00014	69.2	2.52	0.18	po	
		0.0141	0.7054	0.7050	0.00015	70.4	3.04	0.18	po	
KV-280-574.95	OLPX (F)	0.0029	0.7051	0.7050	0.00012	68.8	7.60	0.20	po	
		0.0026	0.7051	0.7050	0.00011	68.4	7.19	0.24	po	
		0.0033	0.7054	0.7053	0.00013	72.8	8.00	0.23	po	
		0.0027	0.7053	0.7052	0.00014	71.9				
KV-297-1236.80	Basal PX	0.0032	0.7058	0.7057	0.00015	59.3	4.00	0.19	po	
		0.0035	0.7051	0.7050	0.00014	60.6	3.57	0.21	po	
KV-103-258.08	OLPX	0.0033	0.7067	0.7066	0.00018	42.2	3.08	0.22	po	
		0.0700	0.7091	0.7071	0.00029	42.4	3.35	0.24	po	
KV-103-303.49	OLPX	0.0130	0.7066	0.7062	0.00021	45.1	-0.42	0.15	py	
		0.0116	0.7074	0.7071	0.00014	46.6	-0.33	0.26	po	
		0.0082	0.7074	0.7072	0.00015	45.1	1.31	0.15	py	
		0.0074	0.7069	0.7067	0.00021	45.5	1.55	0.23	po	
KV-103-421.10	OLPX (R)	0.0089	0.7064	0.7061	0.00023	46.2	4.13	0.24	po	
		0.0111	0.7058	0.7055	0.00024	47.8	5.47	0.26	po	
		0.0127	0.7063	0.7060	0.00022	44.5	3.75	0.20	po	
		0.0069	0.7065	0.7063	0.00021	44.1	3.79	0.20	po	
KV-103-489.30	pOLWB	0.0106	0.7066	0.7063	0.00023	42.7	Core	7.63	0.24	po
		0.0114	0.7078	0.7075	0.00024	42.7	Core	6.98	0.19	po
		0.0103	0.7068	0.7065	0.00028	45.3	Rim	6.99	0.20	po
		0.0127	0.7076	0.7072	0.00027	41.8	Rim	5.84	0.23	po
KV-103-671.18	OLPX* (N)	0.0095	0.7112	0.7109	0.00024	46.6	3.95	0.31	po	
		0.0136	0.7107	0.7103	0.00030	47.6	1.33	0.24	po	
		0.0112	0.7111	0.7108	0.00027	49.5	2.24	0.25	po	

F, R, and N indicate false, regular, and Ni-PGE ore, respectively. Initial  $^{87}\text{Sr}/^{86}\text{Sr}$  ratio  $\pm 2\sigma$  calculated using an age of 2.058 Ga

OLPX olivine pyroxenite, OLPX\* olivine (clino)pyroxenite, pOLWB plagioclase-bearing (ol) websterite, PX pyroxenite, An anorthite, po pyrrhotite, py pyrite



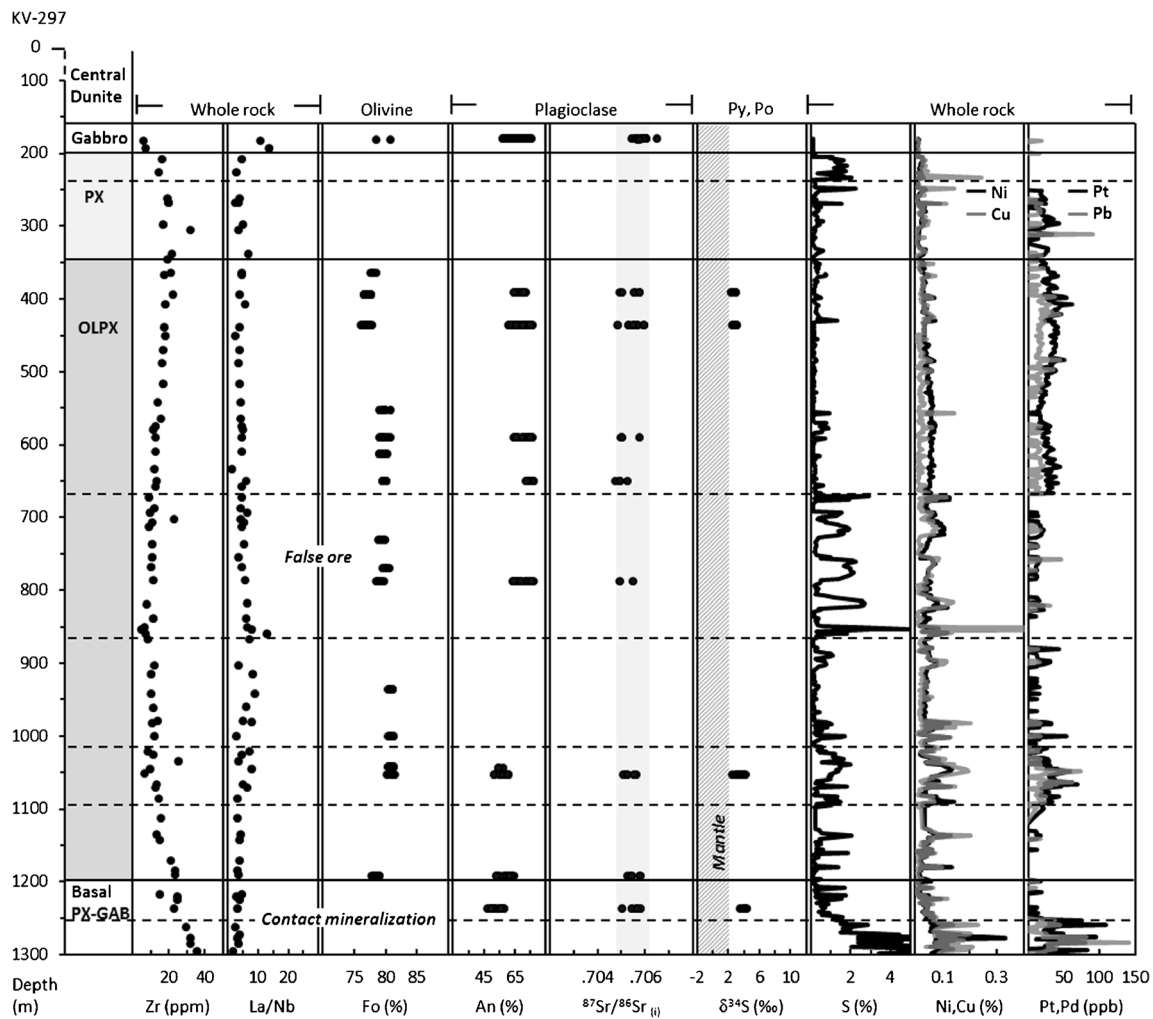


**Fig. 6** Stratigraphic variations of Sr isotope ratios and An contents of plagioclase and S isotope compositions of sulfide in drill core KV-297 (outside the ore domain). The observed range in Sr isotope compositions is depicted by the gray shaded column. Whole-rock Zr, La/Nb, S, Ni, Cu, Pt,

and Pb contents are from the Kevitsa mine database. Fo contents of olivine taken from Luolavirta et al. (2018b) and field for mantle-derived sulfur after Ripley and Li (2003). PX, pyroxenite; OLPX, olivine pyroxenite; basal PX-GAB, basal pyroxenite-gabbro; Po, pyrrhotite; Py, pyrite

lowest  $^{87}\text{Sr}/^{86}\text{Sr}_{(i)}$  ratios ( $\sim 0.7055$ ) in this gabbroic sample (see ESM 3).

**Drill core KV-103 (ore domain)**

In drill core KV-103, representing the ore-bearing domain of the ultramafic zone,  $^{87}\text{Sr}/^{86}\text{Sr}_{(i)}$  varies considerably from 0.7050 to as high as 0.7109 (Fig. 8). The highest Sr isotope ratios, 0.7089–0.7109, were measured from the host rocks to the Ni-PGE ore type, which is consistent with the highly nonradiogenic Nd isotope composition of this ore type (Huhma et al. 2017, in review, Fig. 4). Also a marked peak in La/Nb coincides with the Ni-PGE ore, indicating elevated LREE contents in the host rocks. The mineral compositions and Sr isotope ratios vary widely in the olivine pyroxenites below the pOLWB. The OLPXs above the pOLWB unit are characterized by more uniform Sr isotope ratios of 0.7055 to 0.7073 and a smooth decrease in the An contents of

plagioclase (except for a sharp increase in the uppermost portion of the drill core), but oscillatory variations in the contents of trace elements, such as Zr, and in the olivine compositions. Overall, the  $^{87}\text{Sr}/^{86}\text{Sr}_{(i)}$  values are somewhat higher in comparison to the values obtained for rocks outside the ore domain ( $\sim 0.7047$  to 0.7060). The samples of regular ore yielded initial Sr isotope ratios of 0.7055 to 0.7068, similar to those of the false ore and consistent with the overlap in the initial  $\epsilon_{\text{Nd}}$  values between these ore types (Huhma et al. 2017, in review Fig. 4).

The  $^{87}\text{Sr}/^{86}\text{Sr}_{(i)}$  values within the pOLWB zone show a progressive upward increase, which correlates with a decrease in the An contents of plagioclase and an increase in the Fo contents of olivine. Sample-scale and intragrain variations in  $^{87}\text{Sr}/^{86}\text{Sr}_{(i)}$  are large (Fig. 3d–f, ESM 3). Core to rim traverses across selected plagioclase grains did not reveal any systematic variations in the An content and/or Sr isotope ratio. One sample is an exception where the core domains of individual

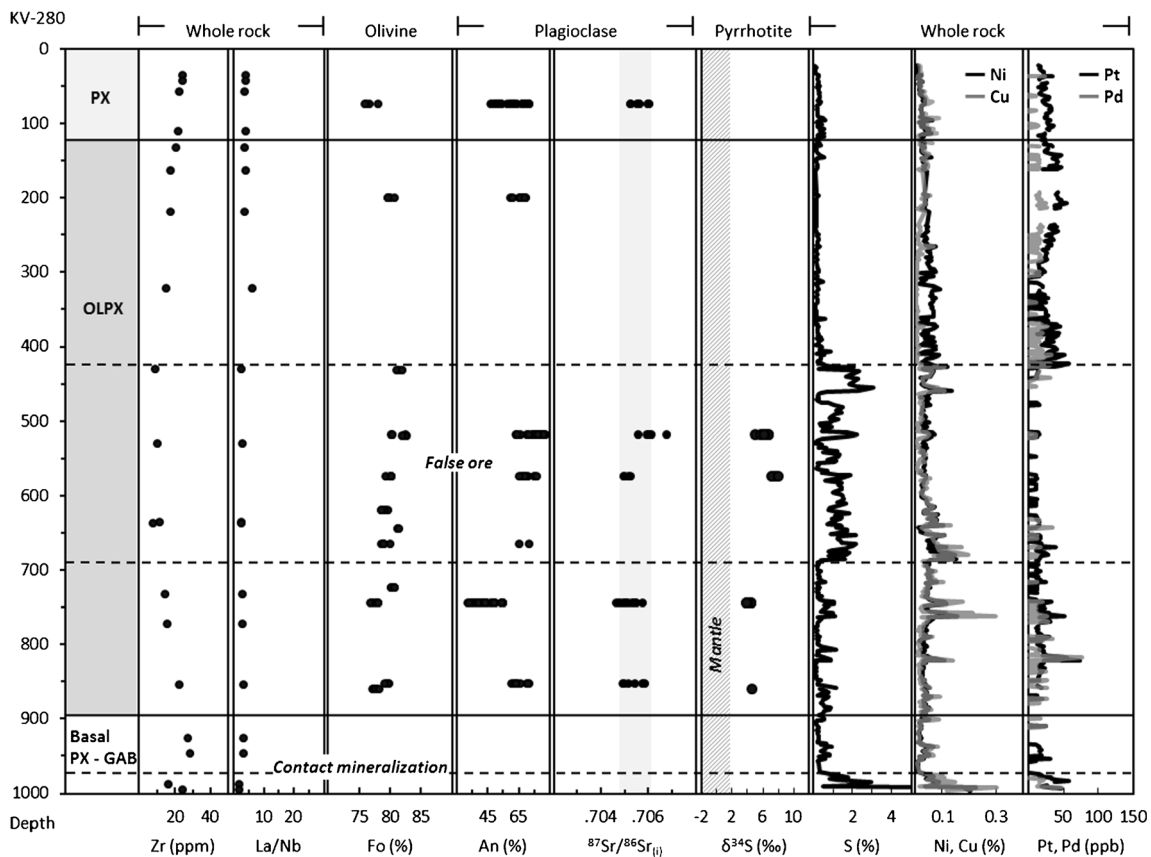


**Fig. 7** Stratigraphic variations of Sr isotope ratios and An contents of plagioclase and S isotope compositions of sulfide in drill core KV-280 (outside the ore domain). The observed range in Sr isotope compositions is depicted by the gray shaded column. Whole-rock Zr, La/Nb, S, Ni, Cu,

Pt, and Pb contents are from the Kevitsa mine database. Fo contents of olivine taken from Luolavirta et al. (2018b) and field for mantle-derived sulfur after Ripley and Li (2003). PX, pyroxenite; OLPX, olivine pyroxenite; basal PX-GAB, basal pyroxenite-gabbro

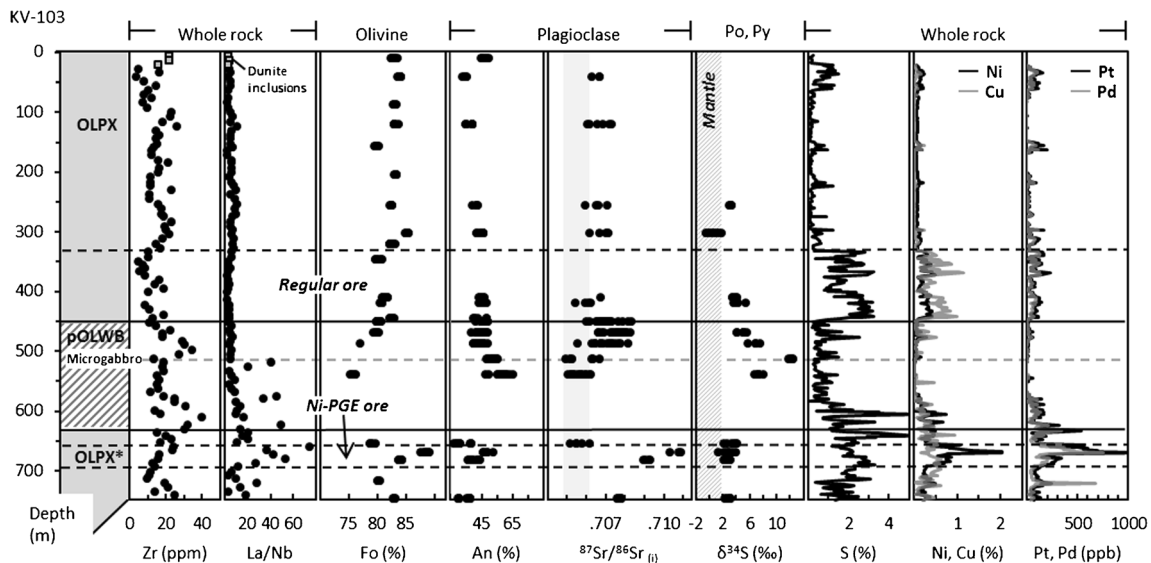


**Fig. 8** Stratigraphic variations of Sr isotope ratios and An contents of plagioclase and S isotope compositions of sulfide in drill core KV-103. Gray shaded column represents the range in Sr isotope compositions observed in drill cores KV-297 and KV-280 (outside the ore domain,

Figs. 4 and 5). Whole-rock Zr, La/Nb, S, Ni, Cu, Pt, and Pb contents are from the Kevitsa mine database. Fo contents of olivine taken from Luolavirta et al. (2018b). OLPX, olivine pyroxenite; \*, olivine (clino)pyroxenite; pOLWB, plagioclase-bearing (olivine) websterite; Po, pyrrhotite; Py, pyrite

grains tend to record the lowest  $^{87}\text{Sr}/^{86}\text{Sr}_{(i)}$  values (KV-103-541.14, see ESM 3), and in this case, it can be postulated that the plagioclase cores represent an early cumulus phase mantled by overgrowths with a variable isotope signature. The microgabbros seem to record two groups of plagioclase with different  $^{87}\text{Sr}/^{86}\text{Sr}_{(i)}$ . However, the small number of analyses may have generated an analytical bias, since distinct ratios were measured from single grain and no correlation between the  $^{87}\text{Sr}/^{86}\text{Sr}_{(i)}$  ratio and An content of that spot can be demonstrated.

A sharp decrease in the Sr isotope ratio at the upper pOLWB-OLPX contact coincides with a minor increase in the olivine Fo contents and the occurrence of ore grades of Ni-Cu sulfides (regular ore).

### In situ S isotope analyses

Sulfur isotope compositions were analyzed for pyrrhotite and, in two samples, also for pyrite. In addition to the different ore types,  $\delta^{34}\text{S}$  values were also measured for sulfides from “barren” rocks with little sulfides. Representative S isotope analyses are listed in Table 1. The whole dataset is provided in Electronic supplementary material 4 (ESM 4) and illustrated in Fig. 5.

### Drill core KV-297 and KV-280 (outside the ore domain)

The false ore samples from drill core KV-280 (outside the ore domain) record a relatively heavy sulfur isotope compositions, with  $\delta^{34}\text{S}$  ranging from +5.1 to +8.0‰ and the median  $\delta^{34}\text{S}$  value being  $\sim$ +6.5‰ (Figs. 5 and 7). For false ore samples, Grinenko et al. (2003) report a wide range of whole-rock  $\delta^{34}\text{S}$  values from +3.4 up to +18.6‰. Most of these whole-rock S isotope data cluster in the range from +5.5 to +11.7‰, being broadly in line with the measured in situ values of this study (Fig. 5). The  $\delta^{34}\text{S}$  values in S-poor samples from drill cores KV-297 and KV-280 range between +2.5 and +6, being generally  $\geq$ +3‰ in the lower parts of these drill cores and  $\leq$ 3‰ higher in the stratigraphy (Figs. 6 and 7).

### Drill core KV-103 (ore domain)

The obtained  $\delta^{34}\text{S}$  values for the regular ore type vary from +3.6 to +5.5‰, with a median of  $\sim$ +4‰, consistent with the previously measured whole-rock  $\delta^{34}\text{S}$  values of +2.0 to +4.6‰ (+3.8‰ on average; Grinenko et al. 2003, Fig. 5). The samples of the Ni-PGE ore type record  $\delta^{34}\text{S}$  values of +1.3 to +4.0‰ with a median value of +2.6‰ (Fig. 5). Interestingly, the obtained in situ  $\delta^{34}\text{S}$  values for Ni-PGE ore are lower than the whole-rock values of +3.0 to +8.8‰ (+6.1‰ on average) reported by Grinenko et al. (2003) (Fig. 5).

The S isotope compositions remain constant in the OLPX below the pOLWB, whereas the mineral compositions and Sr

isotope ratios vary (Fig. 8). In pOLWB, S isotopic compositions are heavy and vary considerably from  $\sim$ +4 up to  $\sim$ +12‰ with stratigraphic fluctuations. The S isotope compositions show mantle-like (from  $-0.4$  to +1.55‰) values at a depth of around 300 m, which coincide with a reversal in the whole-rock Zr contents and is roughly coincidental with the onset of a reversal in olivine composition observed few tens of meters below this depth (see Fig. 8). No correlation exists between the S and Sr isotope compositions.

## Discussion

### Petrogenetic implications for the formation of the Kevitsa ultramafic cumulates

Stratigraphic variations and reversals in mineral compositions and whole-rock element abundances and/or changes in the types and proportions of fractionating minerals are generally considered to indicate open magma chamber processes and periods of magma recharge in igneous rock suites (e.g., Cox and Hawkesworth 1985; Eales et al. 1986, 1990). Radiogenic isotopes (such as Sr) may provide further evidence for such magma chamber processes (e.g., Namur et al. 2010; Liu et al. 2014) by identifying influxes of isotopically different magmas.

This study has shown that compared to the estimated 2.06-Ga depleted mantle or bulk-Earth Sr isotope ratios of 0.7018 and 0.7023, respectively (O’Nions et al. 1979), the calculated  $^{87}\text{Sr}/^{86}\text{Sr}_{(i)}$  values of plagioclase ( $>0.7045$ ) are highly radiogenic throughout the Kevitsa ultramafic cumulates, implying strong involvement of crustal material in their genesis. Similarly, the  $\delta^{34}\text{S}$  values measured for pyrrhotite and pyrite vary from  $-0.42$  to +8.00‰, being generally greater than +2‰ (Fig. 5) and hence heavier than uncontaminated mantle-derived sulfur, which has been estimated to have  $\delta^{34}\text{S}$  values from  $-2$  to +2‰ (Ripley and Li 2003).

The Sr isotope ratios of the Ni-PGE ore (0.709–0.711) are generally much higher than those ( $\sim$ 0.704 to 0.709) obtained by whole-rock (Eales et al. 1990; Lee and Butcher 1990; Kruger 1994; Mitchell et al. 1998) or plagioclase analyses (Seabrook et al. 2005; Yang et al. 2013a; Mangwegape et al. 2016; Wilson et al. 2017) of Lower and Main zone rocks from the Bushveld Complex, which is similar in age to the Kevitsa intrusion (Fig. 4). There are no Sr isotope data on the immediate country rocks or any other rock type from the vicinity of the Kevitsa intrusion to compare with, but Kröner et al. (1981) have published Sr isotope data from the 3.1-Ga Tojottamanselkä gneiss dome located around 10 km north of Kevitsa. At 2.06 Ga, these gneisses had  $^{87}\text{Sr}/^{86}\text{Sr}$  ratios of 0.707–0.711, which overlap the upper part of the  $^{87}\text{Sr}/^{86}\text{Sr}_{(i)}$  range measured for Kevitsa rocks. The similarity of the  $^{87}\text{Sr}/^{86}\text{Sr}_{(i)}$  values suggests that the contaminant end-member

must have had even more radiogenic Sr than that of the ancient gneisses of the Tojottamanselkä dome.

It is worth emphasizing that the Sr isotopes were analyzed using intercumulus plagioclase. It is well-known that the interstitial liquid may percolate within the cumulus pile, and hence, its composition may not directly reflect that of the coexisting cumulus phases (e.g., Boudreau and McCallum 1992; Karykowski and Maier 2017). However, in the case of the Ni-PGE ore, the peculiar features of the silicates (enrichment in LREE, highly radiogenic Sr in plagioclase, highly negative initial whole-rock  $\epsilon_{\text{Nd}}$ , and Ni-rich olivine) as well as the sulfide phase (high Ni tenor) seem to be characteristic for all analyzed samples. In order to preserve these unique features, neither the sulfide liquid nor the intercumulus silicate melt could have migrated extensively with respect to each other or with respect to the cumulus minerals.

### Formation of the “unmineralized” domain of the intrusion

The ultramafic cumulates around the ore domain (drill cores KV-297 and KV-280) show modest fluctuations in whole-rock Zr and olivine Fo contents, rather constant La/Nb ratio, and record predictable fractionation trends from the basal pyroxene-gabbro via olivine pyroxenites to pyroxenites (and gabbro in drill core KV-297) (Figs. 6 and 7). Also, the range of the Sr isotope compositions remains constant throughout the stratigraphy. From the base upwards, reverse fractionation trends can be observed, particularly in the Zr contents. Such marginal reversals are a common feature for mafic intrusive bodies worldwide and are considered to reflect prolonged magma emplacement (Latypov et al. 2011; Egorova and Latypov 2012a, b).

The recent model by Le Vaillant et al. (2017) proposes that the metal-poor sulfide dissemination (false ore) around the ore domain formed within early-stage xenolith-laden sill-like intrusions in which high viscosity circumstances restricted mixing of the magma and sulfide liquid, resulting in low metal tenors. This model is not consistent with the observed homogeneity in the chemical and Sr isotopic compositions of the ultramafic cumulates around the ore domain. We propose that the rocks around the ore domain formed by continuous inputs of chemically and isotopically rather uniform basaltic magma into the Kevitsa magma chamber, followed by crystal fractionation.

The S isotope compositions in false ores are markedly heavier in comparison to “barren” rocks ( $S < 0.5$  wt%). Also the chalcophile metal contents, particularly those of Pt and Pd, as well as the Ni content in olivine (discussed further below) are relatively low. Giving the predictable evolutionary paths and compositional homogeneity of several hundred meter thick succession of olivine pyroxenite in the drill cores located outside the ore domain, the inputs of magma hardly took place

as discrete periods of magma emplacement, yet the metal content and the sulfide budget of the inflowing magma batches varied. Notably, the Sr isotopic compositions remain rather homogeneous throughout the stratigraphy, whereas the S isotopic compositions vary. This is best explained by bulk contamination of the magma at some deep-seated staging chamber and variable degrees of assimilation of crustal sulfur during transportation of the magma into the Kevitsa magma chamber.

### Formation of the ore-bearing domain of the intrusion

The compositional stratigraphy of drill core KV-103 is characterized by obvious fluctuations in the whole-rock Zr contents and olivine compositions and variations in the Sr and S isotope signatures (Fig. 8). Luolavirta et al. (2018b) suggest that the stratigraphic variations in mineral and whole-rock compositions in the drill cores from the ore domain reflect episodes of magma replenishment. The high  $^{87}\text{Sr}/^{86}\text{Sr}_{(i)}$  values (0.709–0.711) in the host rocks to the Ni-PGE ore and their marked decrease at the level of the regular ore further support open magma chamber processes, yet restricted to the ore-bearing domain of the intrusion. The sulfur isotope ratios in drill core KV-103 show no correlation with the Sr isotope compositions, indicating that the magma pulses assimilated variable degrees of silicate components and sulfur from the country rocks or the isotopic signatures were generated via separate contamination processes (as proposed based on isotopic data outside the deposit area in drill cores KV-297 and KV-280).

### Sample-scale Sr isotope heterogeneity and intramineral disequilibrium in pOLWB

Plagioclase-bearing olivine websterites are only found in the ore domain where they form irregular zones that locally act as marker horizon for regular ore-type sulfides (as in drill core KV-103). According to the model by Mutanen (1997), whereby all lithological and chemical variations are a result of variable degrees of in situ contamination, the zones of pOLWB could be interpreted to reflect significant incorporation of pelitic material in their genesis. More recently, the generation of the zones of pOLWB has been related to fractionation of individual magma pulses, with sulfide mineralization occurring near the basal parts of these pulses (Gregory et al. 2011). The obtained Sr isotope ratios show a progressive increase up-hole through the pOLWB, which correlates with a decreasing anorthite content of plagioclase and an increasing Fo content of olivine. Such mineral compositional and isotopic profiles cannot be explained by simple crystal fractionation.

In the pOLWB zones, the sample-scale variations in  $^{87}\text{Sr}/^{86}\text{Sr}_{(i)}$  are relatively large and core-to-rim traverses reveal considerable intramineral isotopic differences (Fig. 3d–f,

ESM 3). Grain-scale isotopic disequilibrium has been explained by interaction of the initial magma with a new, isotopically distinct magma influx (Tepley et al. 2000; Gao et al. 2015), by late-stage infiltration of isotopically distinct residual melt or fluid through the cumulate pile and its reaction with solid crystals in the pile (Chutas et al. 2012; Yang et al. 2013a), or crystallization accompanied by contamination (Templey and Davidson 2003). These processes should result in systematic core-to-rim zonation in isotope compositions of individual grains. Chutas et al. (2012) also observed different Sr isotope compositions between large and small orthopyroxene grains in the Lower Zone of Bushveld Complex and proposed that the larger grains grew at the expense of smaller ones in the presence of fluid with different  $^{87}\text{Sr}/^{86}\text{Sr}_{(i)}$ .

To explain the wide sample- and grain-scale spread of  $^{87}\text{Sr}/^{86}\text{Sr}_{(i)}$  in pOLWB is not straightforward. First of all, we have not observed either clear trends in  $^{87}\text{Sr}/^{86}\text{Sr}_{(i)}$  values between plagioclase cores and rims or any distinct textural populations that record more homogeneous  $^{87}\text{Sr}/^{86}\text{Sr}_{(i)}$  values. Also, no apparent correlation exists between  $^{87}\text{Sr}/^{86}\text{Sr}_{(i)}$  and An, suggesting that the plagioclase crystallized from an isotopically heterogeneous intercumulus liquid. However, it must be noted that the analyzed plagioclase grains are irregular in shape and the actual position of core domains (assumed early cumulate) cannot be accurately defined. The  $^{87}\text{Sr}/^{86}\text{Sr}_{(i)}$  values in the pOLWB zone approach those measured from the underlying OLPX unit hosting Ni-PGE ore, and hence, upward percolation of residual melt originating from the underlying OLPX could be a viable explanation for the radiogenic Sr in the pOLWB. However, in this case, it would be reasonable to expect an opposite sense of isotopic change, i.e., an upward decrease in  $^{87}\text{Sr}/^{86}\text{Sr}_{(i)}$  in the pOLWB. A similar assumption would apply to the interaction (mixing/mingling or melt percolation) between pOLWB with the overlying OLPX.

A concomitant up-hole increase in Mg# of orthopyroxene and initial Sr isotope ratio, similar to that observed in pOLWB zone, has been described from the basal unit of the Lower Main Zone of the Bushveld Complex (Mitchell 1990; Mitchell et al. 1998). It was explained by mixing of resident residual magma in the chamber with new influxes of the Main Zone type, high  $^{87}\text{Sr}/^{86}\text{Sr}_{(i)}$  magma. Progressive mixing or mingling of unsolidified pOLWB and the overlying, more primitive OLPX could potentially explain the reverse fractionation trends in mafic minerals, yet as discussed above, the Sr isotopic profile across the pOLWB-OLPX contact does not indicate any significant interaction between these rock units. It must be noted that the compositions of ferromagnesian minerals may have equilibrated with variable degrees of trapped liquid resulting in modifications in their primary compositions (Barnes 1986). This could potentially explain the up-hole increase in the olivine Fo contents in the pOLWB zone. Petrography or whole-rock compositions of the studied

samples, however, do not reveal any significant differences in the amount of trapped liquid.

In the Rum layered intrusion, Templey and Davidson (2003) observed a trend of upward-increasing plagioclase  $^{87}\text{Sr}/^{86}\text{Sr}_{(i)}$  toward a lithological unit contact, accompanied by isotopic disequilibrium between cores and rims of some grains. The authors propose that the magma from which the plagioclase crystallized underwent progressively larger degrees of in situ contamination. The model predicts that isotopic disequilibrium develops in minerals initially growing near the roof/margins of the intrusion where crustal contamination can be assumed to be most effective. The presence of microgabbros within the zones of pOLWB supports the crystallization of the pOLWB in proximity to the wall rocks. Similar considerations can be inferred from the relatively large variation in the S isotope composition in the pOLWB zones. However, we cannot unambiguously state whether the pOLWB potentially represents a roof sequence of a discrete magma pulse or a separate intrusive phase(s) at the time when the geometry of the Kevitsa intrusion was different from what is currently observed, or autolith(s) of some former marginal-phase rock of the Kevitsa intrusion.

## Implications for ore-forming processes

### Isotopic constraints on the origin of the Ni-Cu-(PGE) ore

Many authors have discussed and reviewed the theoretical aspects related to the formation of magmatic Ni-Cu-PGE deposits (e.g., Naldrett 1999, 2004, 2011; Maier et al. 2001; Arndt et al. 2005; Barnes and Lightfoot 2005; Maier and Groves 2011; Song et al. 2011). Briefly, the key factors include (i) a reasonably high degree of mantle melting generating a parental mafic-ultramafic magma with adequate concentrations of metals; (ii) emplacement of the magma into or onto the crust with minimum prior fractionation of olivine or sulfides; (iii) contamination of the magma with crustal materials, promoting sulfide saturation; (iv) interaction of sulfides with a large volume of magma resulting in enrichment of the sulfides in metals; and (v) mechanical concentration of sulfides to economic levels.

The solubility of sulfide in a mafic magma is known to increase with falling pressure, and hence, magmas ascending to shallow crustal depths are likely sulfur undersaturated (e.g., Mavrogenes and O'Neill 1999). Consequently, a process is required to bring the magma to sulfur saturation under low-pressure conditions. In the case of magmatic Ni-Cu sulfide deposits, this is generally achieved via various processes of contamination, such as addition of silica or volatiles (see Ripley and Li 2013 for a review). Evidently, the most feasible process is incorporation or external sulfur to the magma as evidenced by the nonmantle-like S isotopic signatures of

various sulfide deposits (e.g., Li et al. 2003; Ripley et al. 1999, 2002, 2005; Barnes et al. 2001; Duan et al. 2016).

In this respect, the Kevitsa deposit is not an exception as almost all measured  $\delta^{34}\text{S}$  isotope values in both “barren” and mineralized samples in the Kevitsa ultramafic cumulates exceed +2‰ (Fig. 5), suggesting incorporation of crustal sulfur into the Kevitsa magma. Both the regular and false ore type record heavy S isotope compositions ( $\delta^{34}\text{S}$  averaging +4.0 and +6.5‰, respectively), and hence, external sulfur appears to have been important in the formation of these mineralization styles. For the Ni-PGE ore type, the average in situ  $\delta^{34}\text{S}$  value ( $\sim$ +2.6‰) is only slightly above the assumed mantle values. However, significantly heavier whole-rock  $\delta^{34}\text{S}$  values of +3.7 to +8.8‰ have also been reported (Grinenko et al. 2003), and hence, there might be a substantial internal isotopic variation in these ore zones.

The obtained Sr and S isotope compositions do not show any mutual correlation. In particular, outside the ore domain, the Sr isotopic compositions remain relatively constant throughout the stratigraphy, whereas S isotopes vary significantly (Figs. 6 and 7). As discussed above, this suggests bulk contamination of the silicate magma at depth, followed by selective assimilation of crustal sulfur during the transportation of the magma into the Kevitsa magma chamber. This is in agreement with Grinenko et al. (2003) who reported heavy S isotopic compositions (+18‰ on average) for the immediate sedimentary rocks around the Kevitsa intrusion but noted marked decoupling in the C contents and  $\delta^{13}\text{C}$  values between the Kevitsa ores and sediments. Consequently, they concluded that these sedimentary rocks could not act as the main source of sulfur, and hence, sulfur assimilation took place at a deeper level in the crust.

As discussed above, it is proposed that the ore-bearing domain of the intrusion formed via multiple emplacements of variably contaminated silicate magma and sulfide liquid. Dynamic systems are generally considered favorable for generating economic sulfide deposits because sulfides are able to interact with, and collect metals from, a large volume of magma (e.g., Naldrett 2011). The vigorous emplacement of the ore domain of the Kevitsa intrusion is further supported by the presence of numerous dunitic inclusions and komatiitic xenoliths, highlighting the capacity of intruding magmas to break off fragments from adjacent wall rocks. Recently, Luolavirta et al. (2018a) proposed that the flow rate of the magma decreased due to the entrapment of a large number of inclusions, which aided settling of the sulfide droplets. An alternative view by Le Vaillant et al. (2017) proposes that the regular ores formed under high R factors in an expanded convecting magma chamber.

The origin of the Ni-PGE ore stays enigmatic. Yang et al. (2013b) suggested that assimilation of Ni-rich sulfides from komatiitic xenoliths enriched the magma in Ni, leading to the crystallization of Ni-enriched olivine found in the Ni-PGE ore

and the formation of this ore type. However, they acknowledge that this model fails to explain the peculiar isotopic and REE characteristics of the ore type. The crustal-like isotope compositions of the host rocks to the Ni-PGE ore suggest significant incorporation of crustal material in their genesis. This is in contrast with the primitive mineral compositions as well as the mineralogy of the host rocks (olivine-clinopyroxene cumulates with little or no orthopyroxene), which argue against any excessive role of crustal contamination. The contaminant for the Ni-PGE ore remains unidentified but was likely poor in silica and rich in calcium (and obviously Ni and PGEs) to aid crystallization of Ca-pyroxene rather than orthopyroxene. To generate the markedly distinct chemistry of the Ni-PGE ore in comparison to the regular and false ore, the magma(s) producing the Ni-PGE ore type probably interacted with different country rocks en route to the Kevitsa magma chamber.

The regular and false ore types record similar initial  $^{87}\text{Sr}/^{86}\text{Sr}$  (this study) and  $\epsilon_{\text{Nd}}$  (Huhma et al. 2017, in review), REE characteristics (Hanski et al. 1997; Luolavirta et al. 2018b) as well as a range in the compositions of ferromagnesian minerals. Hence, the parental silicate magmas for the two ore types were likely similar in composition. However, marked differences are observed in the S isotope compositions and metal contents in minerals and rocks, which are discussed in the following chapter.

## Previous sulfide segregation

Olivine Fo-Ni trends are powerful in providing information about the evolution of the magmas and, in particular, their sulfide saturation history (e.g., Li and Naldrett 1999; Li et al. 2004, 2007, 2013; Thakurta et al. 2008). This is due to the fact that in the presence of sulfides, Ni as a highly chalcophile element ( $D^{\text{Ni}} \sim 500$ ; Peach et al. 1990) readily partitions into the sulfide phase, resulting in Ni depletion in the magma and in the olivine crystallized from it. Also, subsolidus Ni-Fe exchange reactions between olivine and coexisting sulfide may modify the primary olivine compositions, producing an inverse olivine Ni-Fo relationship as documented from several magmatic sulfide ore deposits, such as Jinchuan (Li et al. 2004), Noril’sk and Talnakh (Li et al. 2003), and Voisey’s Bay (Li and Naldrett 1999).

In the Kevitsa olivine-pyroxene cumulates, sample-scale variations in the Fo content of olivine are modest ( $\sim$ 1%), but Ni in olivine may vary considerably, resulting in a wide scatter in a Fo vs. Ni plot (Fig. 9). The same is true for the olivine in the Central Dunite and dunite inclusions hosted by the Kevitsa intrusion (Luolavirta et al. 2018a). To model fractional crystallization, theoretical olivine Fo-Ni compositional trends were constructed using the PETROLOG software (Danyushevsky and Plechov 2011). The olivine-melt model (involving  $D^{\text{Ni}}$ ) from Herzberg and O’Hara (2002), the

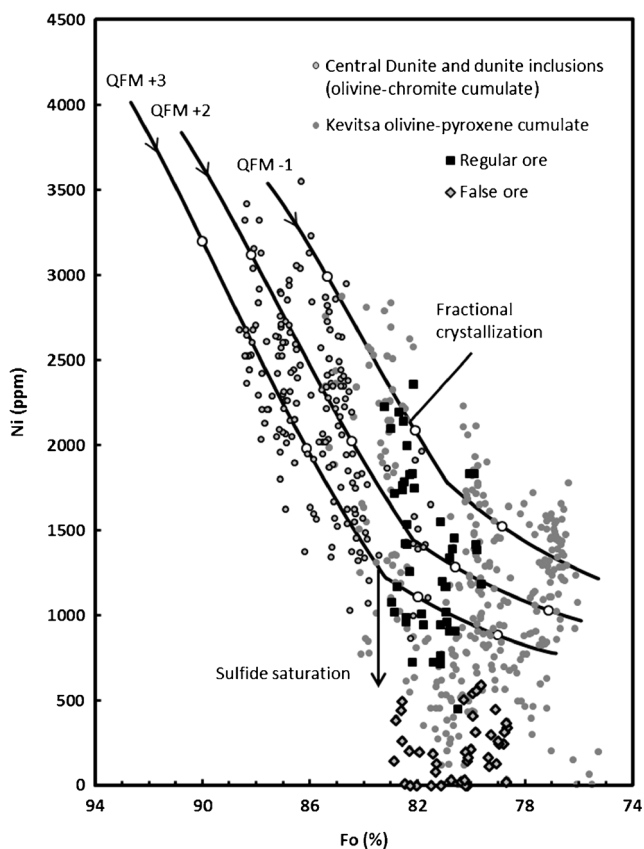


**Fig. 9** Plot of nickel vs. forsterite (Fo %) contents of olivine in dunitic cumulates and Kevitsa olivine-pyroxene cumulates compared with theoretical olivine compositional trends calculated at QFM+3, QFM+2 and QFM-1 for picrite-basalt parental magma. White dots in model curves refer to 10, 20, 30, and 40 percentages of fractional crystallization. Olivine data for dunitic cumulates taken from Luolavirta et al. (2018a) and for Kevitsa olivine-pyroxene cumulates from Luolavirta et al. (2018b)

clinopyroxene-melt model from Danyushevsky (2001), and the clinopyroxene-melt  $D^{\text{Ni}}$  value of 3 (Lindstrom and Weill 1978) were used. A Mg-rich picritic basalt (700 ppm Ni) from the Savukoski Group (Hanski et al. 2001a) is considered parental for the early-stage dunitic cumulates of the Kevitsa intrusive suite (Luolavirta et al. 2018a) and was used as the initial melt composition. The extremely nickeliferous olivines in the host rocks to the Ni-PGE ore were not considered in the calculation. Calculations were conducted under conditions of QFM+3 (three log units above the quartz-fayalite-magnetite  $f\text{O}_2$  buffer), QFM+2 and QFM-1.

The olivine in the host rocks to the false ore is clearly depleted in Ni with respect to the expected Ni contents due to fractional crystallization. Analyses of olivine enclosed in orthopyroxene oikocrysts (isolated from sulfides) in false ore samples record similarly low Ni abundances as olivine grains in contact with sulfides, indicating that the Ni-poor nature of olivine is not due to late-stage equilibration with sulfides. Analogously, Yang et al. (2013b) did not observe any significant differences in the olivine Ni contents between olivine

grains enclosed in clinopyroxene crystals and those in contact with sulfide minerals in the Ni-PGE ore type. Furthermore, we cannot identify any reverse trends in the Ni-Fo relationships that would suggest Fe-Ni exchange reactions. Therefore, the magma producing the olivine in false ore was most likely depleted in Ni due to an early attainment of sulfide saturation.

Given the compositional and isotopic similarity of the host rocks to the regular and false ores, the false ore could represent a differentiation after the formation of economic Ni-Cu ore, explaining the lack of metals in the former. The olivine data from Mutanen (1997) suggest that the forsterite content in olivine in false ore ( $\text{Fo}_{76-78.5}$ ) is overlapping but generally lower than that of the regular ore ( $\text{Fo}_{77-84}$ ). However, our new data on false ores expand the range of Fo in false ores to the range of regular ores. Also, the whole-rock compositions show no difference in the fractionation stage between these two ore types. It must be noted that the dense sulfide liquid may migrate within semiconsolidated cumulates, so that the observed assemblage of silicate and sulfide minerals in false ores do not necessarily represent interrelated accumulations. The different S isotope compositions of the regular and false ore, however, do not favor a simple genetic relationship of the two.

Due to the highly chalcophile nature of platinum group elements ( $D_{\text{PGE}}^{\text{sulfide-silicate}} \sim 20,000$ ; e.g., Fleet et al. 1991), the sulfide segregation history can also be assessed on the basis of the PGE contents and their relative abundances with respect to less chalcophile base metals (e.g., Maier et al. 1998; Barnes and Lightfoot 2005). In false ores, the Pt and Pd concentrations are low in comparison to “barren” olivine pyroxenites (see Figs. 6 and 7) and fall close to or below the detection limit (10 ppb). Such low values may cause large errors in the calculated Cu/Pd or Pt/Pd ratios, for example, and hence, in this case, are not reliable for evaluating the possibility of an earlier sulfide saturation event. Nevertheless, the markedly low concentrations of Pt and Pd in the false ores are well in line with the Ni-depleted nature of the olivine of the ore type, supporting an earlier sulfide segregation event. In this case, to produce metal-poor false ore, the magma must have reached sulfide saturation at two separate stages. The heavy sulfur isotope compositions measured for the false ore indicate a substantial proportion of crustal sulfur, which is consistent with multiple sulfur saturation events.

## Geological model

The different Sr isotope profiles obtained from drill cores outside and within the ore domain cannot be unambiguously correlated. The Sr isotope ratios record a significant variability in the ore domain (see Fig. 8), whereas the surrounding rocks (see Figs. 6 and 7) show less radiogenic and more constant isotope compositions throughout the stratigraphy. Luolavirta et al. (2018b) demonstrate that the lithological, whole-rock, and mineral compositional variations in the stratigraphy are far more

pronounced in the ultramafic rocks of the ore-bearing domain in comparison to the surrounding ultramafic rocks. This is well in line with the observed isotopic signatures. The isotopic and compositional differences can be interpreted to reflect distinct magmatic histories in the ore domain and its surroundings. To explain the spatial stratigraphic and compositional differences between different parts of the Kevitsa intrusion and the characteristic features of the ore types, the following integrated model is proposed for the magmatic evolution of the Kevitsa intrusive suite rocks and its Ni-Cu-(PGE) deposit (Fig. 10).

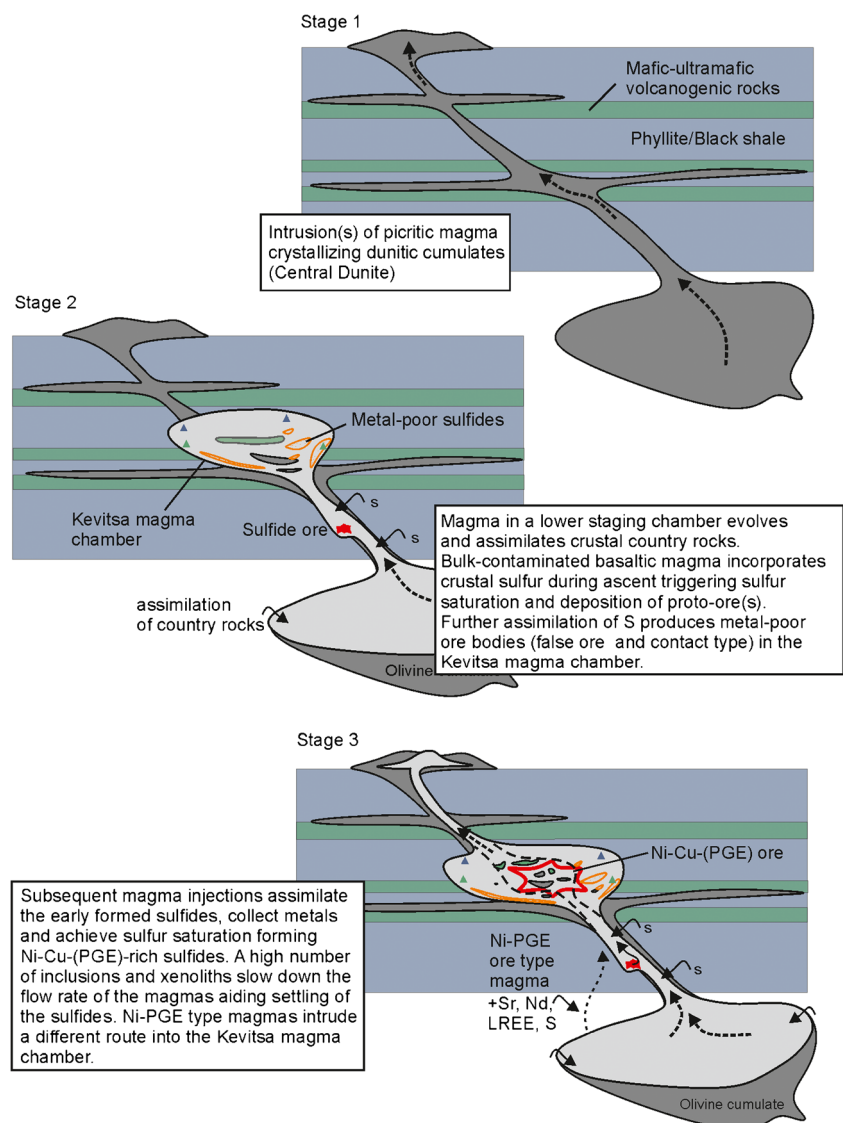
**Stage 1.** Intrusion(s) of picritic basalt magma formed olivine-chromite cumulates (Central Dunite) in the conduits (Luolavirta et al. 2018a).

**Stage 2.** Picritic basalt in a lower staging chamber differentiated to basaltic magma and underwent comprehensive country rock contamination. The basaltic magma intruded as a continuous, stable flow into the Kevitsa magma chamber and crystallized olivine-pyroxene cumulates. During their flow, the

magma pulses assimilated sulfur from country rocks to variable degrees. When sulfur saturation was achieved, some of the sulfides were lodged probably in depressions within the conduit. Metal-depleted magma further gained sulfur from the country rocks and carried sulfide melt into the Kevitsa magma chamber precipitating metal-poor false ores (and contact type mineralization). Later crystal fractionation resulted in the formation of pyroxenites in a nearly closed system.

**Stage 3.** The Kevitsa magma chamber began to operate as a dynamic open system and magmas intruded into the hot interior of the Kevitsa intrusion. A number of stage 1 dunitic cumulates and xenoliths were further brecciated by these magmas and redistributed within the olivine-pyroxene cumulates. The origin of the zones of pOLWB remains ambiguous. They may either represent blocks of separate earlier sill(s) or autolith(s) of some marginal phase rocks formed at stage 2. A simple origin by crystal fractionation involving contamination cannot be ruled out either.

**Fig. 10** Schematic illustration of the emplacement of the Kevitsa intrusive suite rocks and formation of the Ni-Cu-(PGE) ore (modified after Luolavirta et al. 2018b)





Ni-Cu-(PGE) ores formed by sulfur-saturated magma influxes and were potentially upgraded by assimilation of the stage 2 proto-ore material in the conduit. Variable degrees of interaction of the new magma pulses with the early-formed sulfides could account for the wide variation in ore tenors found in the Kevitsa deposit. The magmas producing the Ni-PGE ore likely passed through distinct country rocks and followed a different route into the Kevitsa magma chamber. The numerous dunite inclusions and mafic-ultramafic xenoliths within the deposit area may have reduced the flow rate of the magmas and aided concentration of the sulfides.

## Conclusions

Both strontium and sulfur isotope compositions of the Kevitsa ultramafic cumulates deviate from those expected for purely mantle-derived magmas, indicating involvement of crustal material in their genesis. Variations in the Sr and S isotope data together with mineral and whole-rock chemistry demonstrate that the ore-bearing domain of the Kevitsa intrusion represents a dynamic site with multiple emplacements of variably contaminated silicate magma and sulfide liquid. In contrast, the rocks around the ore domain formed from a compositionally more uniform magma and underwent a less vigorous emplacement history. The sulfur in the Kevitsa ores is at least in part derived from crustal sources, with the external sulfur playing an important role in triggering sulfide saturation. The metal-depleted nature of the false ores and their host rocks indicate previous S saturation and formation of proto-ores during an early stage of magma emplacement. Assimilation of the early formed sulfides may have upgraded the metal tenors of the Kevitsa Ni-Cu-(PGE) ore.

**Acknowledgements** FQM is acknowledged for the access to the company's database and drill cores. The personnel at the Kevitsa mine are kindly thanked for all their assistance during drill core sampling. We are particularly grateful to Shenghong Yang, Markku Lappalainen, Petri Peltonen, Teemu Voipio, and Tommi Lehtilä for discussion and support of the research. We also want to thank Marco Fiorentini and an anonymous reviewer for valuable review and editors Bernd Lehmann and Pasi Eilu for their comments that helped us improve the manuscript. Leena Palmu is thanked for helping with the mineral chemistry analyses.

**Funding information** Financial support for this study was provided by First Quantum Minerals Ltd (FQM) and research grants from the Academy of Finland (grant number 281859), K.H. Renlund Foundation, Tauno Tönning Foundation, and Scholarship Fund of the University of Oulu

## References

- Amdt N, Leshner C, Czamanske G (2005) Mantle-derived magmas and magmatic Ni-Cu-(PGE) deposits. *Economic Geology*, 100th Anniversary Volume, pp 5–24
- Barnes SJ (1986) The effect of trapped liquid crystallization on cumulus mineral compositions in layered intrusions. *Contrib Mineral Petrol* 93(4):524–531. <https://doi.org/10.1007/BF00371722>
- Barnes S-J, Lightfoot P (2005) Formation of magmatic nickel-sulfide ore deposits and processes affecting their copper and platinum-group element contents. *Economic Geology 100th Anniversary Volume*, pp 179–213
- Barnes S-J, Melezhik VA, Sokolov SV (2001) The composition and mode of formation of the Pechenga nickel deposits, Kola Peninsula, northwestern Russia. *Can Mineral* 39(2):447–471. <https://doi.org/10.2113/gscanmin.39.2.447>
- Boudreau AE, McCallum IS (1992) Infiltration metasomatism in layered intrusions—an example from the Stillwater Complex, Montana. *J Volcanol Geotherm Res* 52(1–3):171–183. [https://doi.org/10.1016/0377-0273\(92\)90139-5](https://doi.org/10.1016/0377-0273(92)90139-5)
- Brownscombe W, Ihlenfeld C, Coppard J, Hartshorne C, Klatt S, Siikaluoma JK, Herrington RJ (2015) The Sakatti Cu-Ni-PGE sulfide deposit in northern Finland. In: Maier WD, Lahtinen R, O'Brien H (eds) *Mineral deposits of Finland*. Elsevier, Amsterdam, pp 211–252. <https://doi.org/10.1016/B978-0-12-410438-9.00009-1>
- Chen CJ, Chen B, Li Z, Wang ZQ (2016) Important role of magma mixing in generating the Mesozoic monzodioritic–granodioritic intrusions related to Cu mineralization, Tongling, East China: evidence from petrological and in situ Sr-Hf isotopic data. *Lithos* 248–251:80–93
- Chutas NI, Bates E, Prevec SA, Coleman DS, Boudreau AE (2012) Sr and Pb isotopic disequilibrium between coexisting plagioclase and orthopyroxene in the Bushveld Complex, South Africa: microdrilling and progressive leaching evidence for sub-liquidus contamination within a crystal mush. *Contrib Mineral Petrol* 163(4):653–668. <https://doi.org/10.1007/s00410-011-0691-7>
- Cox KG, Hawkesworth CJ (1985) Geochemical stratigraphy of the Deccan Traps at Mahabaleshwar, Western Ghats, India, with implications for open system magmatic processes. *J Petrol* 26(2):355–377. <https://doi.org/10.1093/petrology/26.2.355>
- Danyushevsky LV (2001) The effect of small amounts of H<sub>2</sub>O on crystallisation of mid-ocean ridge and backarc basin magmas. *J Volcanol Geotherm Res* 110(3–4):265–280. [https://doi.org/10.1016/S0377-0273\(01\)00213-X](https://doi.org/10.1016/S0377-0273(01)00213-X)
- Danyushevsky LV, Plechov P (2011) Petrolog3; integrated software for modeling crystallization processes. *Geochem Geophys Geosyst* 12: Q07021
- Depaolo DJ (1985) Isotopic studies of processes in mafic magma chambers: I. The Kiglapait intrusion, Labrador. *J Petrol* 26(4):925–951. <https://doi.org/10.1093/petrology/26.4.925>
- Duan J, Li C, Qian Z, Jiao J, Ripley EM, Feng Y (2016) Multiple S isotopes, zircon Hf isotopes, whole-rock Sr-Nd isotopes, and spatial variations of PGE tenors in the Jinchuan Ni-Cu-PGE deposit, NW China. *Miner Deposita* 51(4):557–574. <https://doi.org/10.1007/s00126-015-0626-8>
- Eales HV, Marsh JS, Mitchell AA, De Klerk WJ, Kruger FJ, Field M (1986) Some geochemical constraints upon models for the crystallization of the upper critical zone-main zone interval, northwestern Bushveld complex. *Mineral Mag* 50(358):567–582. <https://doi.org/10.1180/minmag.1986.050.358.03>
- Eales HV, De Klerk WJ, Butcher AR, Kruger FJ (1990) The cyclic unit beneath the UG1 chromitite (UG1FW unit) at RPM Union Section Platinum Mine—Rosetta stone of the Bushveld Upper Critical Zone. *Mineral Mag* 54(374):23–43. <https://doi.org/10.1180/minmag.1990.054.374.03>
- Egorova V, Latypov R (2012a) Processes operating during the initial stage of magma chamber evolution: insights from the marginal reversal of the Imandra Layered Intrusion, Russia. *J Petrol* 53(1):3–26. <https://doi.org/10.1093/petrology/egr054>
- Egorova V, Latypov R (2012b) Prolonged magma emplacement as a mechanism for the origin of the marginal reversal of the Fongen-

- Hyllingen layered intrusion, Norway. *Geol Mag* 149(05):909–926. <https://doi.org/10.1017/S001675681200009X>
- Fleet ME, Stone WE, Crocket JH (1991) Partitioning of palladium, iridium, and platinum between sulfide liquid and basalt melt: effects of melt composition, concentration, and oxygen fugacity. *Geochim Cosmochim Acta* 55(9):2545–2554. [https://doi.org/10.1016/0016-7037\(91\)90372-C](https://doi.org/10.1016/0016-7037(91)90372-C)
- Gao JF, Zhou MF, Robinson PT, Wang CY, Zhao JH, Malpas J (2015) Magma mixing recorded by Sr isotopes of plagioclase from dacites of the Quaternary Tengchong volcanic field, SE Tibetan Plateau. *J Asian Earth Sci* 98:1–17. <https://doi.org/10.1016/j.jseaes.2014.10.036>
- Gregory J, Jourmet N, White G, Lappalainen M (2011) Kevitsa copper nickel project in Finland: technical report for the mineral resources and reserves of the Kevitsa project. First Quantum Minerals Ltd
- Grinenko LN, Hanski E, Grinenko VA (2003) Formation conditions of the Kevitsa Cu-Ni deposit, northern Finland: evidence from S and C isotopes. *Geochim Int* 41:154–167
- Hanski E, Huhma H (2005) Central Lapland greenstone belt. In: Lehtinen M, Nurmi PA, Rämö OT (eds) Precambrian bedrock of Finland—key to the evolution of the Fennoscandian Shield. Elsevier, Amsterdam, pp 139–193. [https://doi.org/10.1016/S0166-2635\(05\)80005-2](https://doi.org/10.1016/S0166-2635(05)80005-2)
- Hanski EJ, Huhma H, Suominen IM, Walker RJ (1997) Geochemical and isotopic (Os, Nd) study of the early Proterozoic Kevitsa intrusion and its Cu-Ni deposit, northern Finland. In: Papunen H (ed) Mineral deposits: research and exploration—where do they meet? Proceedings of the fourth biennial SGA meeting, Turku, 11–13 August, 1997. A. A. Balkema, Rotterdam, pp 435–438
- Hanski E, Huhma H, Rastas P, Kamenetsky VS (2001a) The Palaeoproterozoic komatiite-picrite association of Finnish Lapland. *J Petrol* 42(5):855–876. <https://doi.org/10.1093/petrology/42.5.855>
- Hanski E, Walker RJ, Huhma H, Suominen I (2001b) The Os and Nd isotopic systematics of the 2.44 Ga Akanvaara and Koitelainen mafic layered intrusions in northern Finland. *Precambrian Res* 109(1–2):73–102. [https://doi.org/10.1016/S0301-9268\(01\)00142-5](https://doi.org/10.1016/S0301-9268(01)00142-5)
- Herzberg C, O'Hara MJ (2002) Plume-associated ultramafic magmas of Phanerozoic age. *J Petrol* 43(10):1857–1883. <https://doi.org/10.1093/petrology/43.10.1857>
- Huhma H, Hanski E, Kontinen A, Vuollo J, Mänttari I, Lahaye Y (2017) Sm-Nd and U-Pb isotope geochemistry of the Palaeoproterozoic mafic magmatism in eastern and northern Finland. *Geol Surv Finl, Spec Pap* (submitted for publication)
- Karykowski BT, Maier WD (2017) Microtextural characterisation of the Lower Zone in the western limb of the Bushveld Complex, South Africa: evidence for extensive melt migration within a sill complex. *Contrib Mineral Petrol* 172(8):60. <https://doi.org/10.1007/s00410-017-1380-y>
- Keays RR, Lightfoot PC (2010) Crustal sulfur is required to form magmatic Ni-Cu sulfide deposits: evidence from chalcophile element signatures of Siberian and Deccan Trap basalts. *Mineral Deposita* 45(3):241–257. <https://doi.org/10.1007/s00126-009-0271-1>
- Kröner A, Puustinen K, Hickman M (1981) Geochronology of an Archaean tonalitic gneiss dome in northern Finland and its relation with an unusual overlying volcanic conglomerate and komatiitic greenstone. *Contrib Mineral Petrol* 76(1):33–41. <https://doi.org/10.1007/BF00373681>
- Kruger FJ (1994) The Sr-isotopic stratigraphy of the western Bushveld Complex. *S Afr J Geol* 97:393–398
- Latypov R, Hanski E, Lavrenchuk A, Huhma H, Havela T (2011) A 'three-increase model' for the origin of the marginal reversal of the Koitelainen layered intrusion, Finland. *J Petrol* 52(4):733–764. <https://doi.org/10.1093/petrology/egr001>
- Le Vaillant M, Barnes SJ, Fiorentini ML, Santaguida F, Törmänen T (2016) Effects of hydrous alteration on the distribution of base metals and platinum group elements within the Kevitsa magmatic nickel sulphide deposit. *Ore Geol Rev* 72:128–148. <https://doi.org/10.1016/j.oregeorev.2015.06.002>
- Le Vaillant M, Hill J, Barnes SJ (2017) Simplifying drill-hole domains for 3D geochemical modelling: an example from the Kevitsa Ni-Cu-(PGE) deposit. *Ore Geol Rev* 90:388–398. <https://doi.org/10.1016/j.oregeorev.2017.05.020>
- Lee CA, Butcher AR (1990) Scientific communications: cyclicality in the Sr isotope stratigraphy through the Merensky and Bastard reef units, Atok section, Eastern Bushveld Complex. *Econ Geol* 85(4):877–883. <https://doi.org/10.2113/gsecongeo.85.4.877>
- Lehtonen M, Airo ML, Eilu P, Hanski E, Kortelainen V, Lanne E, Manninen T, Rastas P, Räsänen J, Virransalo P (1998) The stratigraphy, petrology and geochemistry of the Kittilä greenstone area, northern Finland: a report of the Lapland Volcanite Project. *Geol Surv Finl Rep Invest* 140 (in Finnish with English summary)
- Li C, Naldrett AJ (1999) Geology and petrology of the Voisey's Bay intrusion: reaction of olivine with sulfide and silicate liquids. *Lithos* 47(1–2):1–31. [https://doi.org/10.1016/S0024-4937\(99\)00005-5](https://doi.org/10.1016/S0024-4937(99)00005-5)
- Li C, Ripley M (2005) Empirical equations to predict sulfur content of mafic magmas at sulfide saturation and applications to magmatic sulfide deposits. *Mineral Deposita* 40(2):218–230. <https://doi.org/10.1007/s00126-005-0478-8>
- Li C, Ripley EM, Maier WD, Gomwe TES (2002) Olivine and sulfur isotopic compositions of the Uitkomst Ni-Cu sulfide ore-bearing complex, South Africa: evidence for sulfur contamination and multiple magma emplacements. *Chem Geol* 188(3–4):149–159. [https://doi.org/10.1016/S0009-2541\(02\)00098-0](https://doi.org/10.1016/S0009-2541(02)00098-0)
- Li C, Ripley EM, Naldrett AJ (2003) Compositional variations of olivine and sulfur isotopes in the Noril'sk and Talnakh intrusions, Siberia: implications for ore-forming processes in dynamic magma conduits. *Econ Geol* 98:69–86
- Li C, Xu Z, de Waal SA, Ripley EM, Maier WD (2004) Compositional variations of olivine from the Jinchuan Ni-Cu sulfide deposit, western China: implications for ore genesis. *Mineral Deposita* 39(2):159–172. <https://doi.org/10.1007/s00126-003-0389-5>
- Li C, Naldrett AJ, Ripley EM (2007) Controls on the Fo and Ni contents of olivine in sulfide-bearing mafic/ultramafic intrusions: principles, modeling, and examples from Voisey's Bay. *Earth Sci Front* 14(5):177–183. [https://doi.org/10.1016/S1872-5791\(07\)60043-8](https://doi.org/10.1016/S1872-5791(07)60043-8)
- Li C, Ripley EM, Thakurta J, Stifter EC, Qi L (2013) Variations of olivine Fo-Ni contents and highly chalcophile element abundances in arc ultramafic cumulates, southern Alaska. *Chem Geol* 351:15–28. <https://doi.org/10.1016/j.chemgeo.2013.05.007>
- Lindstrom DJ, Weill DF (1978) Partitioning of transition metals between diopside and coexisting silicate liquids. I. Nickel, cobalt and manganese. *Geochim Cosmochim Acta* 42(6):817–831. [https://doi.org/10.1016/0016-7037\(78\)90095-9](https://doi.org/10.1016/0016-7037(78)90095-9)
- Liu PP, Zhou MF, Wang CY, Xing CM, Gao JF (2014) Open magma chamber processes in the formation of the Permian Baima mafic-ultramafic layered intrusion, SW China. *Lithos* 184–187:194–208
- Luolavirta K, Hanski E, Maier W, Santaguida F (2018a) Characterization and origin of dunitic rocks in the Ni-Cu ore-bearing Kevitsa intrusion, northern Finland: whole rock and mineral chemical constraints. *Bull Geol Soc Finl*. Online at [http://www.geologinenseura.fi/bulletin/In\\_Press/index.html](http://www.geologinenseura.fi/bulletin/In_Press/index.html)
- Luolavirta K, Hanski E, Maier W, Santaguida F (2018b) Whole-rock and mineral compositional constraints on the magmatic evolution of the Ni-Cu-(PGE) ore-bearing Kevitsa intrusion, northern Finland. *Lithos* 296–299:37–53
- Luukas J, Kousa J, Nironen M, Vuollo J (2017) Major stratigraphic units in the bedrock of Finland, and an approach to tectonostratigraphic division. *Geol Surv Finl Spec Pap* 60:9–40
- Maier WD, Groves DI (2011) Temporal and spatial controls on the formation of magmatic PGE and Ni-Cu deposits. *Mineral Deposita* 46(8):841–857. <https://doi.org/10.1007/s00126-011-0339-6>

- Maier WD, Barnes SJ, De Waal SA (1998) Exploration for magmatic Ni-Cu-PGE sulphide deposits: a review of recent advances in the use of geochemical tools, and their application to some South African ores. *S Afr J Geol* 101:237–253
- Maier WD, Arndt NT, Curl EA (2000) Progressive crustal contamination of the Bushveld complex: evidence from Nd isotopic analyses of the cumulate rocks. *Contrib Mineral Petrol* 140(3):316–327. <https://doi.org/10.1007/s004100000186>
- Maier WD, Li C, De Waal SA (2001) Why are there no major Ni-Cu sulfide deposits in large layered mafic-ultramafic intrusions? *Can Mineral* 39(2):547–556. <https://doi.org/10.2113/gscanmin.39.2.547>
- Malitch KN, Latypov RM, Badanina IY, Sluzhenikin SF (2014) Insights into ore genesis of Ni-Cu-PGE sulfide deposits of the Noril'sk province (Russia): evidence from copper and sulfur isotopes. *Lithos* 204:172–187. <https://doi.org/10.1016/j.lithos.2014.05.014>
- Mangwegape M, Roelofse F, Mock T, Carlson RW (2016) The Sr-isotopic stratigraphy of the Northern Limb of the Bushveld Complex, South Africa. *J Afr Earth Sci* 113:95–100. <https://doi.org/10.1016/j.jafrearsci.2015.10.016>
- Mavrogenes JA, O'Neill HSC (1999) The relative effects of pressure, temperature and oxygen fugacity on the solubility of sulfide in mafic magmas. *Geochim Cosmochim Acta* 63(7-8):1173–1180. [https://doi.org/10.1016/S0016-7037\(98\)00289-0](https://doi.org/10.1016/S0016-7037(98)00289-0)
- Meyer GB, Wilson JR (1999) Olivine-rich units in the Fongen-Hyllingen intrusion, Norway; implications for magma chamber processes. *Lithos* 47(3-4):157–179. [https://doi.org/10.1016/S0024-4937\(99\)00013-4](https://doi.org/10.1016/S0024-4937(99)00013-4)
- Mitchell AA (1990) The stratigraphy, petrography and mineralogy of the main zone of the northwestern Bushveld Complex. *S Afr J Geol* 93:818–831
- Mitchell AA, Eales HV, Kruger FJ (1998) Magma replenishment, and the significance of poikilitic textures, in the lower main zone of the western Bushveld Complex, South Africa. *Mineral Mag* 62(4):435–450. <https://doi.org/10.1180/002646198547783>
- Müller W, Shelley M, Miller P, Broude S (2009) Initial performance metrics of a new custom-designed ArF excimer LA-ICPMS system coupled to a two-volume laser-ablation cell. *J Anal At Spectrom* 24(2):209–214. <https://doi.org/10.1039/B805995K>
- Mutanen T (1997) Geology and ore petrology of the Akanvaara and Koitelainen mafic layered intrusions and the Keivitsa-Satovaara layered complex, northern Finland. *Geol Surv Finl Bull* 395
- Mutanen T, Huhma H (2001) U-Pb geochronology of the Koitelainen, Akanvaara and Keivitsa layered intrusions and related rocks. *Geol Surv Finl Spec Pap* 33:229–246
- Naldrett AJ (1999) World-class Ni-Cu-PGE deposits; key factors in their genesis. *Mineral Deposita* 34(3):227–240. <https://doi.org/10.1007/s001260050200>
- Naldrett AJ (2004) Magmatic sulfide deposits; geology, geochemistry and exploration. Springer, Berlin. <https://doi.org/10.1007/978-3-662-08444-1>
- Naldrett AJ (2011) Fundamentals of magmatic sulfide deposits. *Rev Econ Geol* 17:1–50
- Namur O, Charlier B, Toplis MJ, Higgins MD, Liégeois JP, van der Auwera J (2010) Crystallization sequence and magma chamber processes in the ferrobaltic Sept Iles layered intrusion, Canada. *J Petrol* 51(6):1203–1236. <https://doi.org/10.1093/petrology/egq016>
- O'Nions RK, Evensen NM, Hamilton PJ (1979) Geochemical modeling of mantle differentiation and crustal growth. *J Geophys Res* 84(B11):6091–6101. <https://doi.org/10.1029/JB084iB11p06091>
- Pang K, Li C, Zhou M, Ripley EM (2009) Mineral compositional constraints on petrogenesis and oxide ore genesis of the late Permian Panzihua layered gabbroic intrusion, SW China. *Lithos* 110(1-4):199–214. <https://doi.org/10.1016/j.lithos.2009.01.007>
- Peach CL, Mathez EA, Keays RR (1990) Sulfide melt-silicate melt distribution coefficients for noble metals and other chalcophile elements as deduced from MORB; implications for partial melting. *Geochim Cosmochim Acta* 54(12):3379–3389. [https://doi.org/10.1016/0016-7037\(90\)90292-S](https://doi.org/10.1016/0016-7037(90)90292-S)
- Rankenburg K, Lassiter JC, Brey G (2004) Origin of megacrysts in volcanic rocks of the Cameroon volcanic chain—constraints on magma genesis and crustal contamination. *Contrib Mineral Petrol* 147(2):129–144. <https://doi.org/10.1007/s00410-003-0534-2>
- Ripley EM, Park YR, Li C, Naldrett AJ (1999) Sulfur and oxygen isotopic evidence of country rock contamination in the Voisey's Bay Ni-Cu-Co deposit, Labrador, Canada. *Lithos* 47(1-2):53–68. [https://doi.org/10.1016/S0024-4937\(99\)00007-9](https://doi.org/10.1016/S0024-4937(99)00007-9)
- Ripley EM, Li C, Shin D (2002) Paragneiss assimilation in the genesis of magmatic Ni-Cu-Co sulfide mineralization at Voisey's Bay, Labrador:  $d^{34}\text{S}$ ,  $d^{13}\text{C}$ , and Se/S evidence. *Econ Geol* 97(6):1307–1318. <https://doi.org/10.2113/gsecongeo.97.6.1307>
- Ripley EM, Li C (2003) Sulfur isotope exchange and metal enrichment in formation of magmatic Cu-Ni-(PGE) deposits. *Econ Geol* 98(3):635–641
- Ripley EM, Sarkar A, Li C (2005) Mineralogic and stable isotope studies of hydrothermal alteration at the Jinchuan Ni-Cu deposit, China. *Econ Geol* 100(7):1349–1361. <https://doi.org/10.2113/gsecongeo.100.7.1349>
- Ripley EM, Li C (2013) Sulfide saturation in mafic magmas: is external sulfur required for magmatic Ni-Cu-(PGE) ore genesis? *Econ Geol* 108(1):45–58. <https://doi.org/10.2113/econgeo.108.1.45>
- Rotenberg E, Davis DW, Amelin Y, Ghosh S, Bergquist BA (2012) Determination of the decay-constant of  $^{87}\text{Rb}$  by laboratory accumulation of  $^{87}\text{Sr}$ . *Geochim Cosmochim Acta* 85:41–57. <https://doi.org/10.1016/j.gca.2012.01.016>
- Santaguida F, Luolavirta K, Lappalainen M, Ylinen J, Voipio T, Jones S (2015) The Keivitsa Ni-Cu-PGE deposit in the Central Lapland Greenstone Belt in Finland. In: Maier WD, Lahtinen R, O'Brien H (eds) *Mineral deposits of Finland*. Elsevier, Amsterdam, pp 195–210. <https://doi.org/10.1016/B978-0-12-410438-9.00008-X>
- Seabrook CL, Cawthorn RG, Kruger FJ (2005) The Merensky reef, Bushveld Complex: mixing of minerals not mixing of magmas. *Econ Geol* 100(6):1191–1206. <https://doi.org/10.2113/gsecongeo.100.6.1191>
- Seat Z, Beresford SW, Grguric BA, Waugh RS, Hronsky JMA, Gee MAM, Groves DI, Mathison CI (2007) Architecture and emplacement of the Nebo-Babel gabbro-norite-hosted magmatic Ni-Cu-PGE sulphide deposit, West Musgrave, Western Australia. *Mineral Deposita* 42(6):551–581. <https://doi.org/10.1007/s00126-007-0123-9>
- Seat Z, Beresford SW, Grguric BA, Gee MAM, Grassineau NV (2009) Reevaluation of the role of external sulfur addition in the genesis of Ni-Cu-PGE deposits: evidence from the Nebo-Babel Ni-Cu-PGE deposit, West Musgrave, Western Australia. *Econ Geol* 104(4):521–538. <https://doi.org/10.2113/gsecongeo.104.4.521>
- Song X, Keays RR, Zhou M, Qi L, Ihlenfeld C, Xiao J (2009) Siderophile and chalcophile elemental constraints on the origin of the Jinchuan Ni-Cu-(PGE) sulfide deposit, NW China. *Geochim Cosmochim Acta* 73(2):404–424. <https://doi.org/10.1016/j.gca.2008.10.029>
- Song X, Wang Y, Chen L (2011) Magmatic Ni-Cu-(PGE) deposits in magma plumbing systems: features, formation and exploration. *Geosci Front* 2(3):375–384. <https://doi.org/10.1016/j.gsf.2011.05.005>
- Sparks RS, Huppert HE, Kerr RC, McKenzie DP, Tait SR (1985) Postcumulus processes in layered intrusions. *Geol Mag* 122(05):555–568. <https://doi.org/10.1017/S0016756800035470>
- Tepley FJ III, Davidson JP (2003) Mineral-scale Sr-isotope constraints on magma evolution and chamber dynamics in the Rum layered intrusion, Scotland. *Contrib Mineral Petrol* 145(5):628–641. <https://doi.org/10.1007/s00410-003-0481-y>
- Tepley FJ III, Davidson JP, Clyne MA (1999) Magmatic interactions as recorded in plagioclase phenocrysts of Chaos Crags, Lassen

- volcanic center, California. *J Petrol* 40(5):787–806. <https://doi.org/10.1093/petroj/40.5.787>
- Tepley FJ III, Davidson JP, Tilling RI, Arth JG (2000) Magma mixing, recharge and eruption histories recorded in plagioclase phenocrysts from El Chichon Volcano, Mexico. *J Petrol* 41(9):1397–1411. <https://doi.org/10.1093/petrology/41.9.1397>
- Thakurta J, Ripley EM, Li C (2008) Geochemical constraints on the origin of sulfide mineralization in the Duke Island Complex, southeastern Alaska. *Geochem Geophys Geosyst* 9(7). <https://doi.org/10.1029/2008GC001982>
- Törmänen T, Konnunaho JP, Hanski E, Moilanen M, Heikura P (2016) The Paleoproterozoic komatiite-hosted PGE mineralization at Lomalampi, Central Lapland Greenstone Belt, northern Finland. *Miner Deposita* 51(3):411–430. <https://doi.org/10.1007/s00126-015-0615-y>
- Wilson AH, Armin Z, Gerdes A (2017) In situ Sr isotopes in plagioclase and trace element systematics in the lowest part of the Eastern Bushveld Complex: dynamic processes in an evolving magma chamber. *J Petrol* 58:360–327
- Yang SH, Maier WD, Lahaye Y, O'Brien H (2013a) Strontium isotope disequilibrium of plagioclase in the Upper Critical Zone of the Bushveld Complex: evidence for mixing of crystal slurries. *Contrib Mineral Petrol* 166(4):959–974. <https://doi.org/10.1007/s00410-013-0903-4>
- Yang S, Maier WD, Hanski EJ, Lappalainen M, Santaguida F, Määttä S (2013b) Origin of ultra-nickeliferous olivine in the Kevitsa Ni-Cu-PGE-mineralized intrusion, northern Finland. *Contrib Mineral Petrol* 166(1):81–95. <https://doi.org/10.1007/s00410-013-0866-5>